EINDHOVEN UNIVERSITY OF TECHNOLOGY

Cardiac myofiber reorientation : a mechanism for adaptation?

Citation for published version (APA):
Geerts-Ossevoort, L. (2002). *Cardiac myofiber reorientation : a mechanism for adaptation?* [Phd Thesis 1 (Research TU/e / Graduation TU/e), Mechanical Engineering]. Technische Universiteit Eindhoven. https://doi.org/10.6100/IR555763

DOI:
10.6100/IR555763

Document status and date:
Published: 01/01/2002

Document Version:
Publisher's PDF, also known as Version of Record (includes final page, issue and volume numbers)

Please check the document version of this publication:

• A submitted manuscript is the version of the article upon submission and before peer-review. There can be important differences between the submitted version and the official published version of record. People interested in the research are advised to contact the author for the final version of the publication, or visit the DOI to the publisher's website.
• The final author version and the galley proof are versions of the publication after peer review.
• The final published version features the final layout of the paper including the volume, issue and page numbers.

Link to publication

General rights
Copyright and moral rights for the publications made accessible in the public portal are retained by the authors and/or other copyright owners and it is a condition of accessing publications that users recognise and abide by the legal requirements associated with these rights.

• Users may download and print one copy of any publication from the public portal for the purpose of private study or research.
• You may not further distribute the material or use it for any profit-making activity or commercial gain
• You may freely distribute the URL identifying the publication in the public portal.

If the publication is distributed under the terms of Article 25fa of the Dutch Copyright Act, indicated by the "Taverne" license above, please follow below link for the End User Agreement:

www.tue.nl/taverne

Take down policy
If you believe that this document breaches copyright please contact us at:

openaccess@tue.nl

providing details and we will investigate your claim.

Download date: 22. Aug. 2022

Cardiac myofiber reorientation: A mechanism for adaptation?

CIP-DATA LIBRARY TECHNISCHE UNIVERSITEIT EINDHOVEN

Geerts-Ossevoort, Liesbeth

Cardiac myofiber reorientation: a mechanism for adaptation? / by Liesbeth Geerts-Ossevoort. - Eindhoven : Technische Universiteit Eindhoven, 2002.
Proefschrift. - ISBN 90-386-3003-4
NUR 954
Subject headings: cardiac mechanics ; myofiber structure / cardiac myofiber orientation / cardiac adaptation ; myofibers / cardiac mechanics ; geometry

Druk: Universiteitsdrukkerij TU Eindhoven

Cardiac myofiber reorientation: A mechanism for adaptation?

Proefschrift

ter verkrijging van de graad van doctor
aan de Technische Universiteit Eindhoven,
op gezag van de Rector Magnificus, prof.dr. R.A. van Santen,
voor een commissie aangewezen door het College voor Promoties
in het openbaar te verdedigen op
vrijdag 21 juni 2002 om 13.00 uur

door

Liesbeth Geerts-Ossevoort

geboren te Waalre

Dit proefschrift is goedgekeurd door de promotoren:

prof.dr.ir. M.G.J. Arts
en
prof.dr.ir. D.H. van Campen

Copromotor:
dr.ir. P.H.M. Bovendeerd

Het leven is wat je gebeurt,

terwijl je andere plannen maakt.

Acda & de Munnik

Contents

Summary **xi**

1 Introduction **1**
1.1 General Introduction 2
1.2 Basic cardiac anatomy and physiology 2
1.3 Modeling cardiac mechanics: Importance of myofiber orientation 4
1.4 Adaptation of cardiac geometry
for homogeneity of workload 5
1.5 Cardiac myofiber reorientation: A mechanism for adaptation? . 6
1.6 Aim of the study 7

2 Normal cardiac myofiber orientation in the goat **9**
2.1 Introduction 10
2.2 Methods 12
2.2.1 Diffusion Tensor Imaging 12
2.2.2 Determination of the myofiber direction 13
2.2.3 Determination of an anatomical coordinate system . . . 13
2.2.4 Presentation of the myofiber direction data 13
2.3 Results 17
2.4 Discussion 21
2.4.1 MR-DTI measurements 21
2.4.2 Local coordinate system 22
2.4.3 Normalized transmural position 23
2.4.4 Helix and transverse angle data 23
2.4.5 Divergence of the myofiber field 24
2.5 Conclusion 25
2.6 Acknowledgment 25

3 Active myofiber stress distribution for different cardiac geometries **27**

3.1 Introduction 28
3.2 Methods 29
3.2.1 Description of the model 29
3.2.2 Simulations performed 31
3.2.3 Presentation of simulation results 32
3.3 Results 33
3.4 Discussion 35
3.5 Conclusion 37

4 Myofiber orientation in the infarcted goat heart 39
4.1 Introduction 40
4.2 Methods 41
4.2.1 Animal Model 42
4.2.2 Myofiber orientation 42
4.2.3 Infarct localization 43
4.2.4 Comparison of myofiber orientation in normal and infarcted hearts 44
4.3 Results 45
4.4 Discussion 49
4.5 Conclusion 51

5 Myofiber orientation in the infarct borderzone – a model study 53
5.1 Introduction 54
5.2 Methods 55
5.2.1 Description of the model 55
5.2.2 Simulations performed 58
5.2.3 Presentation of simulation results 58
5.3 Results 59
5.4 Discussion 63
5.5 Conclusion 65

6 General discussion 67
6.1 Introductory remarks 68
6.2 Measurement of myofiber orientation 68
6.3 Animal model 70
6.4 Numerical model of cardiac mechanics 71
6.5 Cardiac myofiber reorientation: A mechanism for adaptation? . 71
6.6 Conclusion 73

References **75**

A Appendix **85**
A.1 Definition of reference myofiber orientation 86
A.2 Active constitutive behavior 86

Samenvatting **89**

Dankwoord **93**

Curriculum Vitae **95**

Summary

The pump function of the heart is generated by the contractile function of the myofibers in the cardiac wall. The contribution of each myofiber to total pump function depends strongly on its orientation. In the normal heart, orientation of myofibers varies smoothly from the inner to the outer cardiac wall over an angle of about 120°.
The normal heart is able to adapt to changes in mechanical load, in order to generate the required pump function. The adaptive process tends to normalize mechanical load in the cardiac wall. It is clear that a change in wall mass or wall mass distribution is one of the adaptive changes that may occur. Other possible adaptive responses might involve changes in material properties, or myofiber orientation.
In the present thesis the hypothesis was tested that reorientation of myofibers provides an adaptive mechanism to maintain optimal mechanical load for these myofibers in the cardiac wall.
A combined approach was chosen, involving both animal experiments and finite element modeling of cardiac mechanics. In the experiments, local mechanical load in the cardiac wall was disturbed by induction of a transmural infarction. Ten weeks after infarct induction the myofiber orientation in the normally perfused region adjacent to the infarction (borderzone) was measured. Comparisons were made with myofiber orientation in corresponding regions of normal hearts. The finite element model was used to estimate the mechanical load in the borderzone region. Moreover, the amount of myofiber reorientation needed to restore homogeneity of mechanical load in the borderzone region was estimated.
Myofiber orientation can be measured reliably only in the *post mortem* state. Thus, a longitudinal study of myofiber reorientation is not possible. To evaluate myofiber reorientation, myofiber orientation in the infarcted hearts had to be compared to a reference of normal myofiber orientation obtained in other hearts. Previous studies on normal myofiber orientation reported large

variations in the distribution of myofiber orientation. Partly, these variations may be attributed to the employed histological technique. Furthermore, the difficulties in defining a local wall bound coordinate system, and in normalizing the transmural position may have contributed to the large variation.
Magnetic Resonance Diffusion Tensor Imaging (MR-DTI) was used to measure the distribution of myofiber orientation (chapter 2). Main advantage of this technique over histological methods is the possibility to measure true 3-dimensional myofiber orientation in the intact *post mortem* heart. Furthermore, to convert the measured absolute myofiber orientations to orientations relative to the cardiac wall, a novel definition of a local coordinate system was introduced. This coordinate system was based upon characteristics of the myofiber field and could be applied objectively, thus avoiding inter-observer variability. Finally, a new normalization technique was applied. The transmural coordinate was normalized relative to the radius at which the myofibers were in plane with the short-axis cross-section. A disadvantage of the used normalization technique is the impossibility to detect offset changes. Using MR-DTI and the novel definition of the wall-bound coordinate system, within a heart, myofiber orientation could be measured with an accuracy of 4.5°, which is better than obtained with histological methods (10°). Between different hearts, fiber orientation coincided within 6° (SD for n=5). This variation is low as compared to variation in published data.
It was investigated whether the large variation in the measured helix angle data, presented in literature, could be explained by biological variation in geometry (chapter 3). In a numerical model of LV mechanics the sensitivity of myofiber stress to changes in geometry and fiber orientation was estimated. It was found that changes in myofiber stress, resulting from variations of LV geometry covering the physiological range, could be compensated by changes in fiber orientation of less than 10°. The large variations as reported in literature cannot be attributed to this adaptation. More likely, the reported variations are related to poor definition of a coordinate system.
The general hypothesis of this thesis was investigated in an animal model (chapter 4). We choose a model of regional infarction in the goat heart to induce a redistribution of local mechanical load. Regional systolic function is known to be impaired in the normally perfused myocardium immediately adjacent to an ischemic region, both in the acute and the chronic phase. After 10 weeks of adaptation, myofiber orientations were measured using MR-DTI. Myofiber orientation was not measured to vary significantly in the normally perfused borderzone adjacent to the infarction.

The latter finding may be explained as follows: 1) myofibers do not have the ability to reorient, or 2) homogeneity of mechanical load in the border zone cannot be reverted by myofiber reorientation, or 3) myofiber reorientation did occur, but the amount of reorientation remained below the level of detection with the MR-DTI technique.
The first possibility, that myofibers cannot reorient, is contradicted by experiments. In a numerical model of cardiac mechanics, it was investigated whether restoration of homogeneity of mechanical load through myofiber reorientation was basically impossible, or whether myofiber reorientation would remain below the level of detection. In the model it appeared that, due to the presence of the infarction, inhomogeneity of transmural active myofiber stress in the borderzone adjacent to the infarction increased from 5 to 15%. This inhomogeneity could be compensated by a rigid body rotation on the order of 10° of the myofibers in transmural patches near the infarct (offset change).
Therefore, it was concluded that myofiber reorientation cannot be ruled out as an adaptive mechanism by which homogeneity of mechanical load is restored in the borderzone of a myocardial infarct. However, for an infarcted region of about 10% of total LV wall mass, the magnitude and characteristics of reorientation needed to restore homogeneity of workload, are near the detection limit of current methods for measuring and analysis of myofiber orientation.

Chapter 1

Introduction

1.1 General Introduction

The heart is a hollow muscular organ that pumps blood through the vascular system for transport of oxygen and nutrients to the tissue and metabolic waste products from the tissue. The heart is able to adapt to changes in mechanical load, in order to generate the required pump function (40). An example of the adaptive capacity of the heart is the growth which is observed in response to a chronically increased workload. After all, increased workload is compensated by a proportional enlargement of both cardiac cavities and walls (athlete's heart) (35).
Cardiac adaptation also plays an important role during heart disease. Heart failure, for instance, is a common syndrome associated with insufficient pump function due to dysfunction of myocytes in the whole heart or in parts of it. The resulting changes in load likely induce adaptation in the affected region and its vicinity. For a long term prediction of the outcome of the disease, and the effect of possible treatment strategies, knowledge about the adaptive mechanisms of cardiac tissue is important. Unfortunately, this knowledge is still incomplete. In this thesis, we investigated the role of reorientation of the muscle fibers in the cardiac wall in cardiac adaptation.

1.2 Basic cardiac anatomy and physiology

The actual pumping force of the heart is generated by the ventricles. The right ventricle maintains the pulmonary circulation, the left ventricle (LV) the systemic circulation. The geometry of the left ventricle can be characterized as a cavity encapsulated by a thick wall (90). The relatively thin-walled right ventricle is connected to the subepicardial layers of the left ventricle and covers about half of the surface of the left ventricle (figure 1.1). The interventricular septum is common to both ventricles. Anatomically, it belongs more to the left ventricle. The epicardial free wall of the left ventricle is smooth. The endocardial wall is irregular, showing many invaginations protruding into the wall up to about 30% of its thickness. This part of the wall is called the trabecular layer. In addition to these trabeculae, the papillary muscles originate from the endocardial wall, supporting the mitral valve leaflets.
The heart wall is largely composed of rod-shaped myocytes. Locally these cells are aligned, thus defining a local myofiber orientation. Across various animal species the pattern of myofiber orientation is quite similar. Subepicardial myofibers follow a left handed helix parallel to the wall. Near the apex these myofibers cross the wall, then following a right handed helical pathway at the

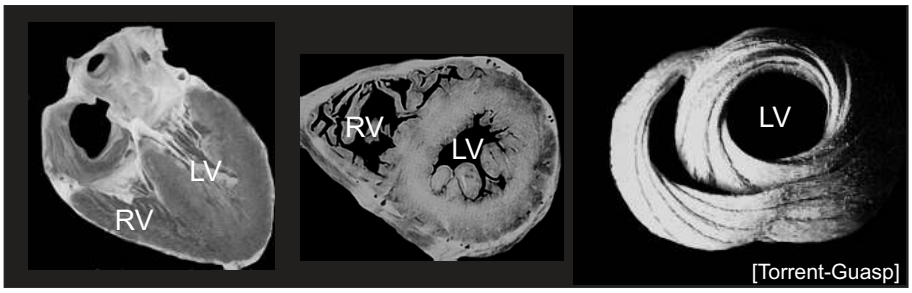

Figure 1.1: *Geometry and myofiber structure of the heart. Left: Long-axis cross-section through the heart, showing the left ventricle (LV) and right ventricle (RV) (Edwards) (32). Middle: Short-axis cross-section through the heart (Edwards) (32). Notice the difference in wall thickness between LV and RV. Right: Apical view on the myofiber structure in the ventricles (Torrent-Guasp) (98). The helical structure has been made visible by blunt dissection of the outer layers.*

subendocardium. Near the base, the myofibers cross over to the subepicardium again. At midwall the myofiber orientation is predominantly circumferential (98) (figure 1.1).

In a closer view myocardial myofibers are locally more or less parallel. Adjacent myocytes are interconnected by numerous bundles of short collagen fibers, called struts (20). These struts likely prevent slipping of adjacent cells in both transverse and lateral directions. The collagen fibers also connect muscle cells to capillaries. Small groups of muscle cells are surrounded by a complex weave of collagen fibers. This weave is tightly coupled to cells which it surrounds (21). Its connections to other weaves are more loose: they are formed by relatively few long collagen fibers. The passive material properties of cardiac muscle tissue are largely determined by the composition and structure of this collagen matrix.

The active pumping force of the heart is generated by contractile units, the sarcomeres, that are arranged in filaments within the muscle cells. Sarcomeres consist of a three-dimensional array of actine and myosine filaments. Upon depolarization of the cell membrane, Ca^{2+} is released, activating the contractile units. As a result the actine filaments slide along the myosin filaments, causing shortening of the sarcomere. Generated stress depends on the time after depolarization, sarcomere length and sarcomere shortening velocity. Myofiber work is directly related to global pump work. The stress generated in the myofibers is responsible for the pressure rise in the left ventricle. Similarly, sarcomere shortening is directly related to the

ejection fraction of the heart. Generally, global cardiac pump function can be characterized by systolic pressure of about 15 kPa and ejection fraction of about 60%.
An important question is how myofiber workload is distributed across the cardiac walls (101). If workload is distributed non-homogeneously, this would imply that regions exist with workload higher than average. These regions could be more susceptible to reduction in blood supply, which would be a risk factor for the development of ischemic heart disease.
In order to investigate the distribution of myofiber workload, both local myofiber stress and strain have to be known. Magnetic Resonance Imaging (MRI) enables non-invasive measurement of three dimensional deformation of cardiac tissue. When local myofiber orientation is known, myofiber strain can be estimated from this tissue deformation. Determination of myofiber stress is more complicated. This stress cannot be measured because insertion of a force transducer damages the tissue (49). Instead, mathematical models, incorporating the features described above, have been developed to estimate the distribution of myofiber stress (6; 9; 14; 23; 24; 42; 50; 51; 52; 68; 106).

1.3 Modeling cardiac mechanics: Importance of myofiber orientation

To investigate the sensitivity of local mechanical load to the distribution of myofiber orientation a numerical model of cardiac mechanics will be used in the present thesis. In the model, only the left ventricle is simulated. Left ventricular endocardial and epicardial surfaces are approximated by truncated confocal ellipsoids. Myofiber orientation is characterized by the helix angle and the transverse angle. The helix angle was defined as the angle between the circumferential direction and the myofiber direction. The transverse angle represented the transmural component of the myofiber orientation. The measured transmural helix angle courses typically ranged from +60 degrees at the subendocardium to -60 at the subepicardium, although a large variation between measurements was found (39; 68; 82; 91; 93). The transverse angle was typically on the order of a few degrees, being positive near the base and negative near the apex (86; 90; 92). Total Cauchy stress in the tissue is the sum of a passive component in the collagen network, and an active component, generated uniaxially in the myofiber direction. The passive component of the tissue stress was modeled nonlinearly elastic, transversely isotropic, and virtually incompressible, as described by Vendelin *et al.* (105). Active stress

was uniaxial, depending on myofiber strain, strain rate and time elapsed after onset of contraction (Appendix A).
Simulations with models of cardiac mechanics have shown that myofiber orientation has a major influence on cardiac wall mechanics (4; 5; 14; 22; 80). In a rotationally symmetric model of LV wall mechanics, similar to the one described above, small variations in the myofiber orientation, within the range of the reported values ($\pm 14°$), resulted in large variations ($\pm 50\%$) of calculated myofiber stress (14). From this it can be concluded that measurements of the distribution of myofiber orientation are not accurate enough to allow reliable estimation of myofiber stress.

1.4 Adaptation of cardiac geometry for homogeneity of workload

Cardiac growth or hypertrophy by adaptation to mechanical load is a frequently studied adaptive mechanism (18; 27; 44; 53; 69). Hypertrophy may occur as a result of long term changes in global or local mechanical loading. Global changes in mechanical loading may occur due to changed hemodynamic load. For instance, in response to pressure overload, the left ventricular wall thickens, whereas the inner diameter remains practically constant (concentric hypertrophy). In response to volume overload the left ventricular wall thickens and the internal diameter increases proportionally (eccentric hypertrophy). Cardiac hypertrophy by adaptation has been shown to result in normalization of the mechanical load in the wall (33; 41; 71). For instance, following concentric or eccentric hypertrophy peak wall stress during systole reverts to normal values (41). Also, in the volume overloaded dog heart adaptive growth appears uniform in fiber and cross fiber directions through the cardiac wall (71). By determining strain along the myofiber direction in the latter study, systolic myofiber shortening appeared practically homogeneous across the wall, both before volume overload and after hypertrophic adaptation. In the rat heart it was found that midwall strains at end diastole were back to normal values after 6 weeks of adaptation to volume overload (33).
Local changes in mechanical load may also induce an adaptation. For instance, after electrical pacing the LV wall is activated asynchronously, resulting in decreased mechanical load near the pacing electrode, and increased load in remote regions. In response, wall mass redistributes i.e., the wall thins near the pacing electrode and thickens in remote regions (77; 102). Also, hypertrophy has been observed in infarcted hearts in regions remote form the infarcted

zone. The degree of hypertrophy correlated to the size of the dysfunctional area (83), and correlated inversely to the circumferential shortening of the myocytes (59).
These findings indicate that local differences in mechanical load induce local differences in tissue growth. Furthermore, adaptive processes tend to normalize mechanical load in the cardiac wall. It is however still unclear what aspects of mechanical load serve as stimulus for adaptation. Several candidates have been proposed, such as stress (61; 81; 95), strain (33; 70; 84), strain or deformation rate (25), and oxygen consumption (29). Similarly, it is still unclear what is limiting adaptive capacity of the cells. Also, much is unknown about the final result of the adaptation process. It is clear that a change in wall mass or wall mass distribution is one of the adaptive changes that may occur, but changes in material properties (74), or myofiber orientation (97), are likely to be involved as well.

1.5 Cardiac myofiber reorientation: A mechanism for adaptation?

In several experimental studies the change in myofiber orientation in response to a change in workload has been investigated. In response to a global change of workload, no alterations in the transmural distribution of myofiber orientation were found (19; 74; 96). However, in several studies in which mechanical load was locally disturbed, indications of changes in local myofiber structure have been found. Tezuka *et al.* showed that right ventricular hypertrophy induced by pressure loading is accompanied by a change in myofiber orientation in the RV anterior outflow tract (97). In chronically paced dog hearts, regions of myofiber disarray were observed (2; 56). Also, at the boundaries of a myocardial infarction dispersion of myofiber orientation was reported (66; 88; 109). Furthermore, at the boundaries of a myocardial infarction structural changes (30; 31; 73) and changes in cell-cell contact and cell-extracellular matrix contact (63) were reported.
Adaptive tissue growth appears to normalize mechanical workload in the cardiac wall. Similarly, in several models of cardiac mechanics it has been assumed that cardiac myofiber orientation is designed such that mechanical load is uniform throughout the cardiac wall. Peskin (75) was able to predict the main characteristics of cardiac myofiber orientation in a model study using the assumption of uniform myofiber stress distribution. Rijcken *et al.* (79; 80) optimized myofiber orientation such that myofiber shortening throughout

the cardiac wall was distributed uniformly and found the optimum to be within the range of anatomical measurements. Since biological optimization mechanisms generally have a local physiological basis, Arts *et al.* (4) developed a numerical model simulating local adaptation of cardiac myofiber orientation and sarcomere length to local mechanical load. After adaptation myofiber orientation closely agreed with experimental data (4; 82; 90).

1.6 Aim of the study

As shown above, it was found in experimental studies that myocardial tissue adapts to changes in mechanical loading. Myofiber reorientation is likely to be involved in the adaptive process. Moreover, mathematical models of cardiac mechanics have demonstrated a high sensitivity of local wall mechanics to myofiber orientation. In view of these findings, myofiber reorientation might be a powerful adaptive mechanism.
The aim of the present study was therefore to investigate the hypothesis that myofiber reorientation in the cardiac wall provides an adaptive mechanism to maintain an optimal mechanical load for the myofibers in the cardiac wall.
To investigate myofiber reorientation, myofiber orientation present under normal circumstances has to be used as a reference. Large variation between measurements of the transmural course of the helix angle was reported (figure 1.2). The lack of accuracy can partly be attributed to the employed histological technique. Recently a technique called Magnetic Resonance Diffusion Tensor Imaging (MR-DTI) has been developed to measure the diffusion tensor for water in biological tissues (7; 8). The principal direction of the diffusion tensor, corresponding to the direction of largest diffusivity, coincides with the myofiber direction (28; 46; 47; 86). As compared to histologic methods, the main advantage of MR-DTI is that myofiber directions are determined truly three-dimensionally in the intact heart. In Chapter 2, we apply the MR-DTI technique to measure the distribution of normal myofiber orientation more accurately than before to create a reference data set. Special attention was paid to the definition of a reproducible coordinate system, attached to the cardiac wall.
In Chapter 3 we investigated whether the large variation in the measured helix angle data (39; 68; 82; 90; 93), presented in literature, may be attributed to biological variations in geometry. In a numerical model of LV mechanics the sensitivity of myofiber stress to changes in geometry and fiber orientation was estimated.

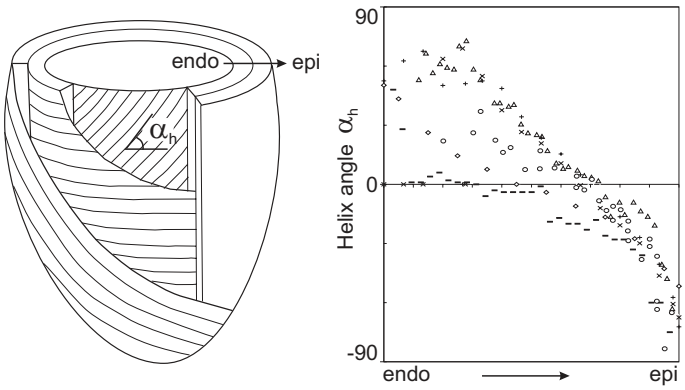

Figure 1.2: *Left: Schematic representation of myofiber orientation in the left ventricular wall. The helix angle α_h is indicated. Right: Different transmural distributions of the helix angle as measured by: ⋄ Streeter (93), - Greenbaum et al. (39), △ Ross et al. (82), + Streeter (90), × Streeter (90) and, ∘ Nielsen (68).*

In Chapter 4 and 5 the hypothesis that myofiber reorientation in the cardiac wall provides an adaptive mechanism to keep mechanical load optimal was tested.

In Chapter 4, we choose a model of regional infarction in the goat heart to induce a redistribution of local mechanical load. Regional systolic function is known to be impaired in the normally perfused myocardium immediately adjacent to an ischemic region, both in the acute (65; 76) and the chronic phase (58). After 10 weeks of adaptation, myofiber orientations were measured using MR-DTI. To detect myofiber reorientation, myofiber orientations as measured in the regions adjacent to the infarction were compared to those in corresponding regions in healthy controls.

In Chapter 5, a mathematical model of LV mechanics was used to simulate the effect of an infarct on changing workload in the vicinity of the infarct. Furthermore, it was evaluated whether homogeneity of myofiber stress could be restored by variation of myofiber orientation in this region.

Chapter 6 contains a discussion of the findings and general conclusions.

Chapter 2

Normal cardiac myofiber orientation in the goat

Characterization of the normal cardiac myofiber field in goat measured with MR Diffusion Tensor Imaging.
L. Geerts, P. Bovendeerd, K. Nicolay and T. Arts
In Press American Journal of Physiology

Cardiac myofiber orientation is a crucial determinant of the distribution of myocardial wall stress. Myofiber orientation is commonly quantified by helix and transverse angles. Accuracy of reported helix angles is limited. Reported transverse angle data are incomplete.
We measured cardiac myofiber orientation post mortem in 5 healthy goat hearts using MR-Diffusion Tensor Imaging. A novel local wall bound coordinate system was derived from the characteristics of the fiber field.
The transmural course of the helix angle corresponded to data reported in literature. The mean midwall transverse angle ranged from $-12^\circ \pm 4^\circ$ *near the apex, to* $+9.0^\circ \pm 4^\circ$ *near the base of the left ventricle, which is in agreement with the course predicted by Rijcken et al using a uniform load hypothesis (80).*
The divergence of the myofiber field was computed, which is a measure for the extent to which wall stress is transmitted through the myofiber alone. It appeared to be <0.07 mm^{-1} *throughout the myocardial walls, except the fusion sites between left and right ventricle and the insertion sites of the papillary muscles.*

2.1 Introduction

Within the cardiac wall, muscle fibers are oriented in a characteristic helix like pattern, which is similar across various animal species. Streeter *et al.* (91; 93) were the first to quantitatively characterize the cardiac myofiber field. Since then, myofiber orientation was measured by Ross (82), Greenbaum (39) and more recently by Nielsen *et al.* (68). For quantification of fiber orientation, the helix and transverse angle have been introduced by Streeter (90). The helix angle represents the longitudinal component of the fiber orientation, whereas the transverse angle represents the transmural component of the fiber orientation. Measured transmural helix angle courses typically range from +60 degrees at the subendocardium to -60 degrees at the subepicardium, although a large variation between measurements exists. Data on the transverse angle are incomplete, stating only that it is typically on the order of a few degrees, being positive near the base and negative near the apex (90; 92).
According to mathematical models of cardiac wall mechanics the distribution of myofiber orientation within the cardiac wall is the main determinant of the distribution of stress and myofiber shortening throughout the wall during ejection (4; 5; 14; 22). Small variations in the fiber orientation, within the range of the reported values ($\pm 10^\circ$), resulted in large variations ($\pm 50\%$) of calculated myofiber stress (14). Therefore, it was concluded that the accuracy of the present methods to quantify fiber orientation was not sufficient to

estimate local myofiber load.
Accuracy of measured myofiber orientation data is limited by several causes. Partly, the lack of accuracy can be attributed to the employed histological technique. Although in a well-cut slice the in-plane fiber orientation can be measured accurately, a possible out-of-plane component remains unknown. This severely affects the accuracy with which the transverse angle can be measured. Typically, the resulting accuracy of histological techniques is limited to about 10° (82; 93), and the best volume resolution obtained is about 10 mm^3 (68).
An other issue in the quantitative description of the fiber orientation is the ambiguity in the definition of a local wall bound coordinate system. Irregularities in the shape of the cardiac wall, such as the presence of papillary muscles and trabeculations at the endocardial wall, hamper the definition of a local coordinate system.
The purpose of this study is to more accurately assess three-dimensional cardiac myofiber orientation by applying Magnetic Resonance Diffusion Tensor Imaging (MR-DTI) and a novel definition of the local coordinate system.
MR-DTI has been developed to measure the diffusion tensor for water in biological tissues (7; 8). In validation studies performed in muscular tissues, it was shown that the principal direction of the diffusion tensor corresponding to the largest diffusivity, is statistically similar to the myofiber direction (28; 46; 47; 86). Also, the technique has been used to reconstruct the fiber orientation in one rabbit heart (87), and a human heart *in vivo* at low resolution (78; 100). However, quantitative results have not been reported. Compared to histologic methods the main advantage of MR-DTI is that true 3-dimensional myofiber direction vectors are determined in the intact heart, with respect to the well determined magnet coordinate system.
In order to obtain an unambiguous definition of the local coordinate system, it was investigated whether such a coordinate system could be defined based upon the characteristics of the myofiber field. Myofiber orientation was measured and quantified by the transmural course of the helix angle and the apex-to-base course of the midwall transverse angle, using a novel definition of the local coordinate system. Fiber orientation between several normal hearts was compared.
Furthermore we have evaluated the divergence of the myofiber orientation field, which was suggested to be close to zero in a study by Peskin *et al* (75). The divergence value may be elevated in regions where irregularities in the cardiac fiber field occur, such as the attachment of the right ventricle and the papillary muscles.

2.2 Methods

The study was performed on 5 healthy female goats weighing 26-55 kg that were sacrificed for unrelated orthopedic experiments. After an overdose of Euthasate the goats were bled to death. The chest was opened and the heart was rapidly excised and rinsed in cold saline. After the removal of the atria the ventricles were weighed. Thereafter, the heart was cast in a 20% gelatin substance, in order to maintain its shape, and subsequently stored at $4°C$. Before measurement, the samples were allowed to adjust to room temperature of $20°C$. MR Diffusion Tensor Imaging measurements were performed within 3 days.

2.2.1 Diffusion Tensor Imaging

^1H MR-DTI measurements were performed in a 4.7 Tesla magnet, interfaced to a Varian (Palo Alto, USA) NMR Spectrometer. The instrument was equipped with a gradient insert (inner diameter 12 cm) that provided a maximal gradient strength of 220 mT m^{-1} with a rise time of 500 μs. Bore temperature was maintained at $20°C$. The gelatin-cast heart was wrapped in plastic foil and placed in a birdcage RF coil in the center of the magnet. The long axis of the left ventricle was visually aligned with the center line of the magnet bore. Diffusion-weighted images were collected with a pulsed field gradient, spin-echo MRI sequence (89), in which the dephasing lobe of the read-out gradient was applied immediately prior to the data acquisition window to minimize cross-talk between the imaging gradients and the diffusion-sensitizing gradients (60). Diffusion weighting was provided using a pair of unipolar rectangular gradient pulses with a duration of δ=15 ms and a separation of Δ=35 ms. Echo time TE was 70 ms, repetition time TR was 4 seconds. Diffusion data were measured in 3 mm thick adjoining slices. The number of slices varied with heart size and was between 19 and 25. The field-of-view of 100 $\times$ 100 mm was represented with an image of 128 $\times$ 128 pixels, resulting in a pixel size of 0.78 $\times$ 0.78 mm^2. Diffusion gradients were applied in 10 directions, optimized according to Jones *et al.* (54). For each direction, 2 different magnitudes of the sensitizing gradient were applied. The strength of these gradients has been optimized according to Jones *et al.* (54), which implies that one measurement with minimal diffusion weighing was followed by another measurement in which approximately 66% of the signal vanished. In our experiments Jones' condition was met with b-values of 0 and 1763 s/mm^2. Two averages were acquired in a total measurement time of about 2.5 hours.

2.2.2 Determination of the myofiber direction

For each diffusion direction Apparent Diffusion Coefficients (ADC's) were determined in each pixel. The ten ADC maps thus derived were used to calculate the tensor components of the diffusion tensor in a least squares approach. Since ADC values typically range from 0.1×10^{-3} to 2.2×10^{-3} mm^2/s, the latter value being the diffusivity measured in free water, ADC values outside this interval were considered unrealistic and were excluded from further analysis. The eigenvector corresponding to the largest eigenvalue of the diffusion tensor was considered to be the myofiber orientation, quantified with respect to the magnet coordinate system. The reliability of the calculated myofiber orientation was assessed by the degree of anisotropy of the diffusion tensor, as quantified by the Fractional Anisotropy (FA), as introduced by Basser *et al.* (8). The FA value indicates the fraction of the diffusion that may be attributed to anisotropic diffusion.

2.2.3 Determination of an anatomical coordinate system

To quantify fiber orientation in terms of the commonly used helix and transverse angle, a transformation from the global magnet coordinate system to the anatomical coordinate system of the heart was performed (figure 2.1). The normal to the imaging plane was taken as a first estimate of the local long axis direction. In each slice the pixels corresponding to myofibers with an out-of-plane component smaller than $\pm$ 0.1 π rad (about 5.7°) were selected, as a first estimate of the midwall region. A best fit circle through these pixels was calculated, yielding a first estimate of the center of the LV in that slice. Next, the local long axis direction was determined as the best fit line through the centers of the LV cross-sections in 5 adjoining slices. The local myofiber orientation was re-evaluated with respect to the new estimate of the local long axis direction. Thus a new set of midwall myofiber pixels was found. Again, a circle was fitted to these pixels to yield the true LV center in a slice. This center served as the origin of a local cylindrical coordinate system along the local anatomical long axis. The direction with angle $\Phi = 0$ was defined along the anterior right ventricular (RV) fusion site. Thus, the image plane may be tilted in the local cylindrical coordinate system.

2.2.4 Presentation of the myofiber direction data

For each goat heart, fiber orientations were measured in 50,000 voxels typically. Since it is impossible to show all data, a selection was made to illustrate

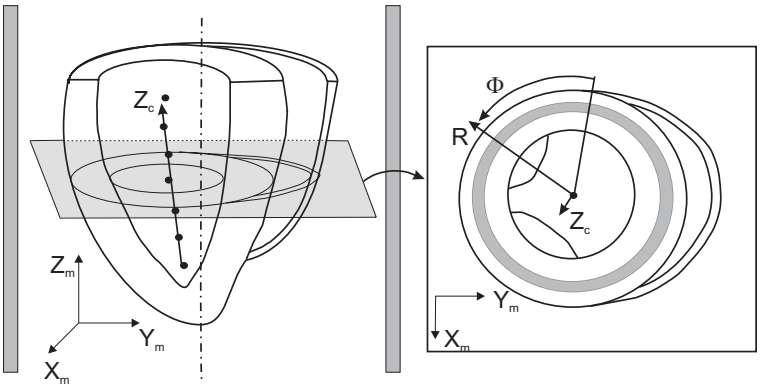

Figure 2.1: *Definition of the local cylindrical coordinate system (R, Φ, Z_c) relative to the rectangular magnet coordinate system (X_m, Y_m, Z_m). The axis Z_c is aligned with the centers of the nearby short axis cross-sections. The angle $\Phi = 0$ indicates the anterior connection of the RV free wall to the LV. In the right figure the pixels corresponding to myofibers with an out-of-plane component smaller than $\pm$ 0.1 π rad are indicated by the gray area.*

the main characteristics of the fiber field. The helix angle was evaluated at several sectors in the equatorial LV short axis slice. The transverse angle was determined in the midmyocardial free wall for all slices from apex to base and averaged over the circumference. Furthermore, the divergence of the fiber field was calculated at each voxel.

Selection of the equatorial slice

The equatorial slice was defined as the slice that was positioned at one-third of the long axis length from the base of the heart (93). The base of the heart was defined as the slice nearest to the outflow tract but not showing it. The apex was the first slice showing cardiac tissue.

Helix Angle

The definition of the fiber direction is ambiguous, since flipping the fiber direction by 180° results in the same fiber direction. Therefore, the vector defining fiber orientation was selected such that the circumferential component was always positive. The helix angle, $\alpha_h^\star$, was calculated as the angle between the myofiber direction and the plane perpendicular to the local long axis direction (figure 2.2). The transmural course of the helix angle was determined for anterior, inter-papillary muscle, posterior and septal sectors, each sector

being 20° wide (figure 2.3). The radius $R_0(\Phi)$, at which the helix angle changes sign was determined for each region using a 5th order polynomial fit through the data. This radius was used to normalize transmural position, R:

$$h = \frac{R - R_0}{R_0} \tag{2.1}$$

where h is the normalized transmural coordinate. For all sectors in each heart the slope of the transmural course of the helix angle was determined using a linear fit to the transmural data for the compact portion of the wall, defined as h>-0.3. To characterize the average helix angle course of all five hearts, helix angle data were grouped and a polynomial fit was determined in all 4 sectors. The papillary muscles were excluded based upon visual inspection, and the endocardial radius was determined. The normalized endocardial position, h_{endo}, could then be calculated using the above mentioned equation.

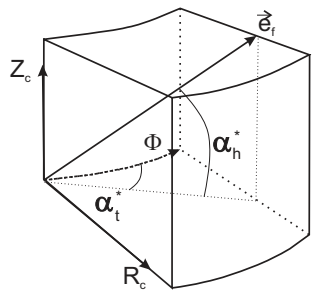

Figure 2.2: *Block of cardiac tissue as taken from the wall to show definition of helix angle, $\alpha_h^\star$, and transverse angle, $\alpha_t^\star$.*

Midwall transverse angle

The transverse angle is the angle by which the cardiac myofibers cross the wall from epicardium to the endocardium. The transverse angle, $\alpha_t^\star$, was defined as the angle between the local circumferential direction and the projection of the fiber direction on the plane normal to the local long axis direction (figure 2.2). In all slices from apex to base this angle was determined in the free wall at $R = R_0(\Phi)$, where the free wall is defined as the LV region spanned between the RV fusion sites (figure 2.3). The transverse angle was averaged over the circumference of the left ventricular free wall. The apex-to-base length was scaled from 0 at the apex to 1 at the base.

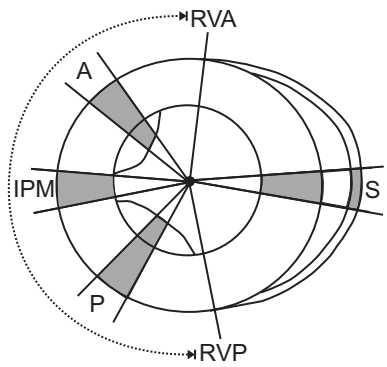

Figure 2.3: *LV sectors used for analysis of the helix angle data. A: Anterior, IPM: Inter-papillary muscle, P: Posterior and S: Septum. RVA: Anterior RV fusion site, RVP: posterior RV fusion site. The LV free wall is the region between RVA and RVP, as indicated by the dotted line.*

Geometry

LV geometry was characterized by the mean radius, R_m, at which the helix angle changes sign. This radius was determined in all slices from apex to base. Apex-to-base length, L_{ab}, was approximated by the distance between the basal and apical slice. Furthermore, the mean wall thickness of the equatorial slice, WT, was determined. For this analysis the papillary muscles were excluded.

Statistical analysis

To investigate whether the range and the slope of the transmural helix angles are different in the different sectors, a multiple-sample comparison was performed. An ANOVA table was constructed, and an F-test was performed to evaluate whether there was a statistically significant difference between the means of the variables at the 95% confidence level. If so, a multiple range tests was performed, using Fisher's least significant difference (LSD) procedure, to assess which mean values are mutually significantly different. The order of the polynomial fits applied to the data was determined using an ANOVA analysis for the coefficients of the polynomial in the order fitted.

Divergence of the fiber field

Peskin (75) showed that, from the quasi-static momentum equilibrium equations, it can be derived that the divergence of the cardiac fiber field is zero, using the following assumptions: 1) during ejection active stress is the

most important determinant of cardiac stress, 2) active stresses are mainly uniaxial, 3) myofiber stress distribution is uniform throughout the wall, 4) the hydrostatic pressure gradient is oriented perpendicular to the fiber direction. To investigate to which extent these assumptions hold in the real heart, we computed the magnitude of the divergence of the fiber field on a pixel-by-pixel basis as in equation 2.2.
We described the fiber field by unit vectors $\overrightarrow{e_f}$, where $[u, v, w]$ represent the components with respect to the $[x, y, z]$ magnet coordinate system. The magnitude of the divergence (MD) of the fiber field was defined as:

$$MD = |\overrightarrow{\nabla} \cdot \overrightarrow{e_f}| = |\frac{\partial u}{\partial x} + \frac{\partial v}{\partial y} + \frac{\partial w}{\partial z}| \tag{2.2}$$

The divergence of the fiber field can be interpreted as a measure of structural continuity of the myofiber field. The requirement that the divergence of the fiber field is zero is the translation of the assumption that the cross-sectional area of a fiber remains constant (75). In other words, every myofiber that enters a voxel must also leave this voxel again.

2.3 Results

General geometric characteristics of the hearts are summarized in table 2.1. Total left and right ventricular mass, M, of the ventricles was 129.2 ± 48.8 g (mean ± sd) . The mean equatorial radius, R_m, and the mean apex-to-base length, L_{ab} of the LV's were 18.5 ± 2.4 mm and 59.4 ± 8.9 mm respectively.

	R_m [mm]	L_{ab} [mm]	$\frac{L_{ab}}{R_m}$ [-]	M [g]	WT [mm]
Heart 1	17.04	54	3.17	89.0	10.27
Heart 2	17.09	54	3.17	97.5	11.60
Heart 3	16.23	51	3.14	94.5	10.12
Heart 4	20.77	69	3.32	185.0	12.84
Heart 5	21.27	69	3.24	180.0	12.65
MEAN	18.5	59.4	3.20	129.2	11.5
SD	2.4	8.9	0.07	48.8	1.3

Table 2.1: *Table summarizing the most important global properties of the heart: LV radius R_m at the equator, apex-to-base length, L_{ab}, the ratio of L_{ab} over R_m, mass of the ventricles, M, and mean wall thickness of the equatorial slice, WT. The ratio of L_{ab} over R_m characterizes heart shape.*

The out-of-plane component of the fiber orientation in the equatorial plane as well as the projection of the fiber orientation onto the plane are visualized in figure 2.4. More axially oriented fibers are found near the epi- and endocardium, and in the papillary muscles. Midwall fibers run predominantly in circumferential direction. At the posterior RV fusion site there is a smooth transition of in-plane fibers from the LV to the RV. At the anterior RV fusion site this transition is more abrupt.

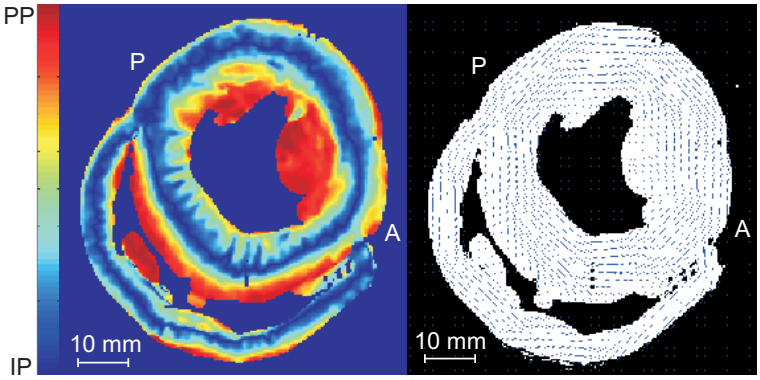

Figure 2.4: *Visualization of the cardiac fiber field in an equatorial slice. Left: Out-of-plane component of the fiber direction. Blue colors indicate in-plane (IP) fiber direction, red colors indicate fiber direction perpendicular to the plane (PP). Right: Projection of the fiber direction onto the imaging plane. P and A indicate posterior and anterior LV free wall.*

The transmural course of the helix angle, as shown in figure 2.5, typically ranges from $+90°$ to $-75°$ at the anterior site, from $+85°$ to $-55°$ at the inter papillary muscle site, from $+80°$ to $-40°$ at the posterior site and from $+50°$ to $-85°$ at the septal site.
The range of the helix angles was largest in the anterior sector and significantly smaller in the posterior sector (table 2.2). The slope of transmural course of the helix angles is steeper in anterior and septal sectors than in posterior and inter papillary muscle sectors. In all sectors, except for the septal sector, a contribution of the papillary muscles is visible as a plateau of $90°$ fibers. In the subepicardial layers of the anterior and septal sectors a steep slope is observed. Within a heart, myofiber orientation was measured with an accuracy of $4.5°$. Consecutively, transmural helix angle data of all five hearts were grouped and fitted using a 5th order polynomial, which resulted in an optimum fit in view of model complexity and statistical significance of the coefficients. The standard

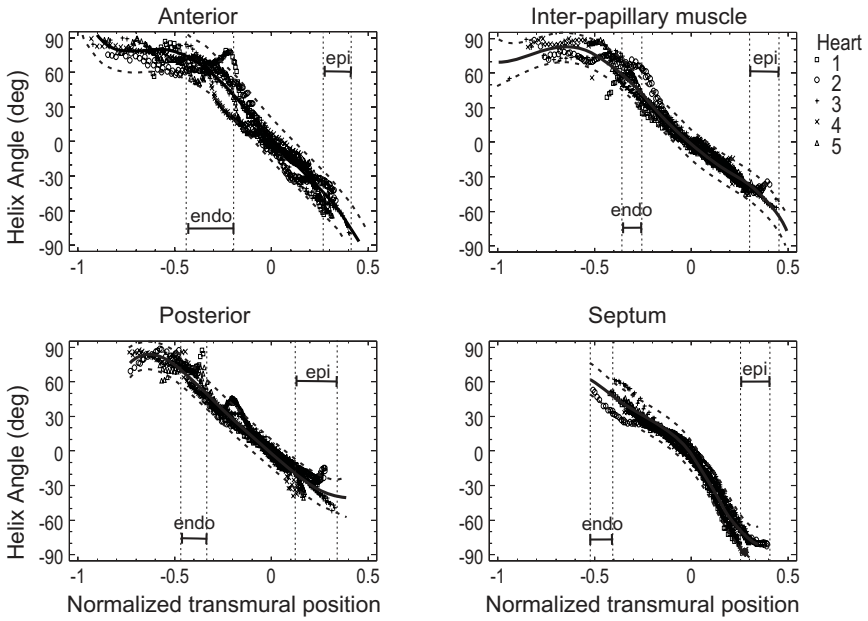

Figure 2.5: *Transmural course of the helix angle in the equatorial slice of all five hearts (symbols). In order to limit the number of data points in the graphs, the sector width was 5°. A 5th order polynomial fit was applied to the data, showing the average HA course (solid line) and the 95 % confidence intervals for predicted values (dashed lines). The normalized endocardial position h_{endo}, as determined from the divergence plots, is indicated in the figures by the vertical dotted lines. Papillary muscle tissue is found left of these lines. Upper left: Anterior sector, Upper Right: Inter papillary muscle sector, Lower Left: Posterior sector, Lower Right: Septum.*

deviation in myofiber orientation thus observed was on the order of $\pm$ 6° in all sectors (figure 2.5).

The transverse angle varies from apex to base as shown in figure 2.6. Using a third order polynomial fit to the data, the mean transverse angle course varied from $-12° \pm 4°$ near the apex, to $+9° \pm 4°$ near the base of the heart. The change of sign of the transverse angle occurred between equator and base of the heart. The apex-to-base course of R_m (figure 2.6) was best described by an elliptical course. The mean equatorial radius appeared to be 19 mm.

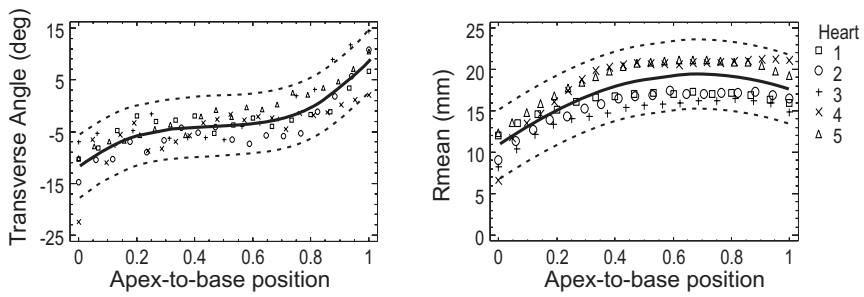

Figure 2.6: *Left: Transverse angle course from apex to base. Right: Mean radius at which the helix angle changes sign, R_m, as a function of apex-to-base position. Solid lines indicate average course, dashed lines indicate 95 % confidence intervals for predicted values.*

	Range (°)				**Slope** (°)			
	S	A	IPM	P	S	A	IPM	P
Heart 1	148.7	153.0	111.0	121.9	-193.8	-197.9	-139.3	-113.9
Heart 2	113.6	177.8	163.5	78.5	-156.0	-186.7	-137.2	-113.9
Heart 3	143.9	179.3	161.1	147.6	-190.8	-196.5	-135.6	-149.0
Heart 4	157.3	142.8	126.0	128.9	-201.4	-147.8	-124.1	-146.3
Heart 5	130.4	173.4	140.5	134.0	-181.8	-173.5	-144.1	-185.3
MEAN	138.8	165.3	140.4	122.2	-184.8	-180.5	-136.0	-141.7
SD	17.1	16.4	22.5	26.2	17.5	20.7	7.4	29.6
			⋆				⋆	

Table 2.2: *Range (°) and slope (°) of the transmural helix angle course as a function of normalized wall position in all equatorial sectors: A; anterior, IPM; Inter papillary muscle, P; posterior and S; septum. Pairs of statistically significant different mean values are indicated (⋆ = P<0.05). The range of anterior and posterior sectors is significantly different. The slopes of anterior and septal sectors are similar, and statistically significantly different from the slopes at the posterior and inter papillary muscle sectors. The slopes of the posterior and inter papillary muscle sectors are similar.*

The divergence of the myofiber field was less than 0.07 mm^{-1} in the major part of the myocardial walls, but significantly exceeded this level at the anterior fusion of the right and left ventricular walls, and at the insertion sites of the papillary muscles (figure 2.7).

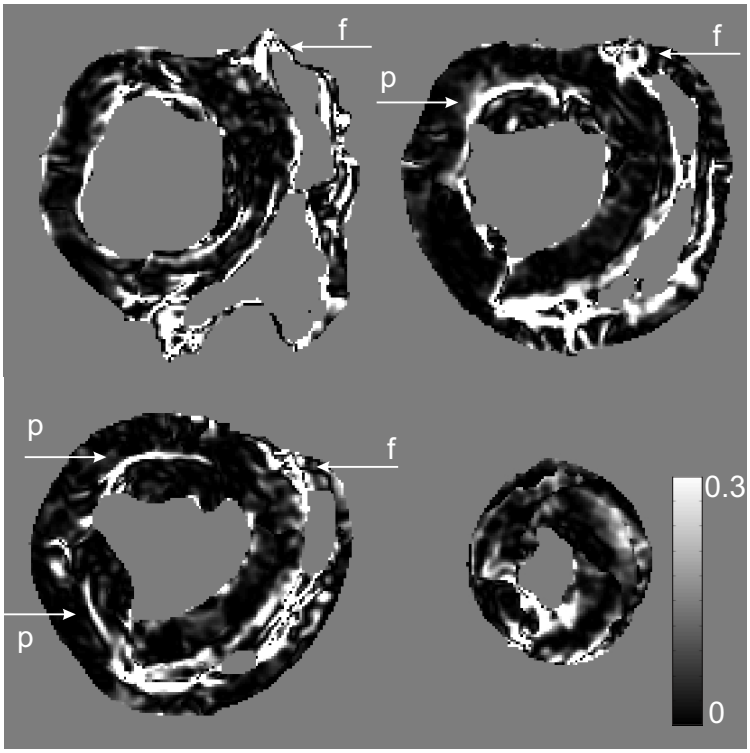

Figure 2.7: *Divergence plots, in which black indicates low divergence values and white indicates divergence > 0.3* mm^{-1}*. Upper left: Basal slice, Upper right: Equatorial slice, Lower left: Slice in middle between apex and equator, Lower right: Apical slice. Arrows indicate the papillary muscle (p) and RV-fusion (f) regions, where the divergence values are significantly higher than 0.07* mm^{-1}*.*

2.4 Discussion

2.4.1 MR-DTI measurements

Fiber orientation has been measured *post mortem* in 5 goat hearts using MR-DTI. Less than 2% of the ADC values was excluded from the data. Values

for the Fractional Anisotropy as found in literature for fresh myocardial tissue range from 0.17 to 0.65 (36; 47; 78). Our value of 0.35 ± 0.03, is well within this range, indicating that the fiber direction was well determined. Most MR-DTI measurements were performed within 4 hours after excision of the heart. We compared the Fractional Anisotropy (FA) values of hearts that were measured immediately after excision, and those that were measured after 3 days. The FA values appeared not to be significantly different between both groups, implying that the structures that are responsible for the diffusion anisotropy are still intact 3 days after excision.
Typically, in one heart fiber orientation was measured in about 50,000 voxels with voxel size of 1.8 mm^3, which is an enhancement in volume resolution as compared to histological measurement techniques by a factor of 5. Regionally, the long axis direction was defined by the direction of a line through center points of the left ventricle in the nearby slices. The transmural coordinate was normalized unambiguously using the radius at which the helix angle changes sign, R_0. Myofiber orientations have been characterized by the helix and transverse angles. Standard deviations for helix angles measured in individual hearts were in the order of $\pm 4.5°$, which is better than the $\pm 10°$ obtained in histological measurements.

2.4.2 Local coordinate system

In the present study the transverse and helix angles were defined with respect to a local cylindrical coordinate system (figure 2.1) instead of the more common wall coordinate system, which consists of a local longitudinal, transmural and circumferential direction (68; 93). In the equatorial slice these coordinate systems coincide. The determined equatorial helix angle data are therefore directly comparable to measurements by other investigators.
Outside the equatorial slice the transverse fiber angle at R_0 in the cylindrical coordinate system, $\alpha_t^\star$, and in the wall coordinate system, α_t, are related as:

$$\alpha_t = \arctan(\tan(\alpha_t^\star)\cos(\beta)) \tag{2.3}$$

where β is the angle between the local longitudinal direction and the local long LV axis. At the equator, where $\beta = 0$, the definitions of α_t and $\alpha_t^\star$ match, but further towards the apex and base their difference increases. Estimating the angle β from the apex-to-base course of R_m (figure 2.6), maximum differences between the two angles were on the order of 2° in the most apical slice and on the order of 1° in the most basal slice.

Errors in the determination of the local long axis direction affect calculation of the helix and transverse angle. Near the apex, local geometry is practically spherical. As a consequence near the apex, determination of the local long axis direction is inherently ill-defined and sensitive to errors. Further away from the apex the long axis direction is well determined, with maximally expected alignment errors between the true LV long axis and our estimation of about $\pm 10°$. Alignment errors of $10°$ result in a maximal offset of the calculated helix angle course by a similar amount. The influence of errors in long axis determination on calculated transverse angles roughly follows the behavior as described by equation 2.3, where β now represents the misalignment error. This implies that for misalignment errors in the order of $\pm 10°$, the error in the transverse angle is as little as about 2% of the calculated $\alpha_t^\star$.

2.4.3 Normalized transmural position

Usually the transmural position is normalized to the local wall thickness. However, determination of wall thickness is difficult due to the presence of papillary muscles and endocardial trabeculations, which hampers detection of the endocardial wall (82; 93). Instead of normalization using the endocardial wall, the radius at which the helix fiber angle equals zero, R_0, is much better defined and has a smooth appearance. Therefore, R_0 was used as a reference radius to which all transmural distances were normalized in this study. Recognition of common patterns between different hearts is therefore enhanced using this normalization technique.
In order to compare our normalization method with the commonly used method, the transmural course of the fiber orientation normalized between endocardium and epicardium was also calculated. The endocardial wall was determined from the divergence plots, where the papillary muscles could be detected. The standard deviation to the helix angle data of the five hearts determined in this manner appeared to be $11°$, which is considerably more than the $6°$ found using our normalization method.

2.4.4 Helix and transverse angle data

Our data on the helix angle are within the range of earlier reported measurements and model predictions (4; 39; 68; 79; 82; 90; 91; 93). To the authors best knowledge, these are the first detailed measurements of the transmural component of muscle fiber direction as a function of the longitudinal position. Earlier studies reported values at only a few longitudinal

positions, often averaged across the wall thickness. For comparison with these data, we assume a parabolic transmural course of the transverse angle, with zero angle at the endo- and epicardium. Then our midwall value equals 1.5 times the transmural average value. Near the apex, the average transmural angle was measured to be $-4.5°$ (90), which is lower than our averaged value of $-7.8°$. Halfway between apex and equator, literature (90) and our values are similar, equalling $-3.5°$ and $-3°$, respectively. Averaged over the subequatorial region, a midwall value of $-8.0°$ has been reported (92), which compares reasonably with our value of $-6°$. Averaged throughout the whole heart we obtain a value of $-3°$, which is considerably lower than the value of $-7.9°$ obtained by Scollan *et al.* This may be due to the fact that in our analysis the most apical slices were left out, since determination of the long axis was considered to be inaccurate. In the apical slices however, the highest values for the transverse angle are expected. Finally, the transverse angle course that we measured compares well to the optimization prediction by Rijcken *et al.* (16; 80).

It has been assumed that myofiber orientation adapts such that local stresses and strains are distributed uniformly throughout the heart (75; 79; 80). Employing this condition in a mathematical model, fiber orientation can be optimized to obtain homogeneous fiber shortening during ejection (80). The resulting optimum orientation was found to be well determined, indicating that variation of fiber orientation in between hearts may be small. This finding was confirmed by the present study.

2.4.5 Divergence of the myofiber field

As shown by Peskin, the assumption that tissue loads are mainly transmitted by the active fibers, each fiber bearing the same load, can be converted to the condition that the divergence of the fiber field is zero. In our study, the divergence of the fiber field is less than 0.07 mm^{-1} throughout the myocardium and significantly elevated at the insertion sites of the papillary muscles and at the anterior RV fusion site. Thus, calculation of the divergence may enable detection of the papillary muscle structures.

However, we found that it was not possible to evaluate stress uniformity on the basis of our measurements, since it can be shown that an active stress inhomogeneity of 10 % results in a divergence value of about 0.005 mm^{-1}. In order to detect these small differences, an accuracy of about $0.3°$ is necessary, which greatly exceeds the current $6°$ accuracy.

2.5 Conclusion

The myofiber structure offers an excellent base for the definition of a cardiac coordinate system. This coordinate system can be based upon the local long axis direction and the transmural coordinate normalized using the radius at which the helix angle changes sign, R_0. With respect to this coordinate system, helix and transverse angles can be defined to characterize the fiber field.
The transmural course of the helix angle we found compares well to earlier measurements. The slope of the transmural helix angle course is largest at the anterior and septal sites. The apex-to-base course of the transverse angle varies according to a 3rd order polynomial, with values of $-12°$ at the apex and $+9°$ at the base.
Both the transmural course of the helix angle and the apex-to-base course of the transverse angle that we measured correspond well to model predictions based on uniformity of stress and strain.
The divergence of the myofiber field appeared to be <0.07 mm^{-1} in the major part of the myocardial walls, except for sharp transitions at the fusion sites between left and right ventricle and at the insertion of the papillary muscles. The accuracy with which the measurement has been performed is not good enough to allow evaluation of uniformity of the stresses.

2.6 Acknowledgment

The authors gratefully acknowledge the technical assistance of Hans Vosmeer and Boudewijn van der Sande.

Chapter 3

Active myofiber stress distribution for different cardiac geometries

L. Geerts, R. Kerckhoffs, P. Bovendeerd, T. Arts

Recently, mathematical models of cardiac mechanics have developed into a stage where they can be adapted to describe the patient's specific situation. However, not all parameters needed in such a model can be measured specifically, so they have to be taken from a default. In order to estimate the possible errors by introducing default values for parameter settings, sensitivity of the model to the actual choice of these parameters must be evaluated.
In the present study we addressed the question whether myofiber stress can be estimated reliably using a default setting for myofiber orientation, to be incorporated into different cardiac geometries.
Cardiac wall mechanics were described with a numerical model. A default myofiber orientation was chosen such that myofiber stress was distributed approximately homogeneous across the wall in a representative geometry. The sensitivity of the calculated stress distribution to changes in geometry was evaluated.
The distribution of myofiber stress within the wall of the left ventricle (LV) appeared to be sensitive to shape of the LV. Geometry variations covering the biological range changed active myofiber stress by maximally 10%. In a more spherical geometry the calculated midwall myofiber stress decreased relative to this stress in the inner and outer layers. In a cylindrical geometry these changes were opposite.

3.1 Introduction

In assessing local cardiac function, both stress and strain are relevant. Magnetic Resonance Imaging (MRI) enables non-invasive measurement of three dimensional deformation of cardiac tissue. Myofiber strain can be estimated from tissue deformation using an estimate of myofiber orientation has. Determination of myofiber stress is more complicated. This stress cannot be measured because insertion of a force transducer damages the tissue (49). Instead, mathematical models have been developed to estimate the distribution of myofiber stress (6; 9; 14; 23; 24; 42; 106).
Whereas early simple mathematical models were used to investigate basic aspects of cardiac mechanics, more recently models have developed into a stage where they can be adapted to describe the patient's specific situation. With a patient specific model, abnormalities in the cardiac deformation pattern, as detected with MR tagging, may be analyzed to deduct the underlying pathology. In models of cardiac mechanics many parameters have to be known. In designing a patient specific model of cardiac mechanics one has to decide

which sets of parameters will be measured specifically and which ones will be taken from a default. Data on geometry may be derived from high resolution MR images. Other data, for instance on electrical activation sequence or myofiber orientation, cannot be determined easily for each patient specifically. Then a default setting may be preferred. In order to estimate the possible errors resulting from default values for parameter setting, the sensitivity of the model to the actual choice of these parameters must be evaluated.
In the present study we address the question whether myofiber stress can be estimated reliably using a default setting for myofiber orientation, to be incorporated into the specific measured geometry of the individual heart.
To solve this question cardiac wall mechanics were described with a numerical model. The sensitivity of the calculated stress distribution to changes in geometry was evaluated in simulations having a fixed distribution of myofiber orientation in different wall geometries. Furthermore it was investigated whether the resulting redistribution of myofiber stress could be reverted by a compensatory change in the transmural course of myofiber orientation. For this purpose the sensitivity of the myofiber stress distribution was evaluated for two types of changes in the transmural course of myofiber orientation: 1) changing the slope of the transmural course of the myofiber angle, and 2) addition of an offset to the myofiber angle.

3.2 Methods

3.2.1 Description of the model

The left ventricular (LV) endocardial and epicardial surfaces were approximated by truncated confocal ellipsoids. The geometry was defined by wall volume V_w, cavity volume V_{lv}, a common focal length of the ellipsoids C, and the height h, above the equator at which the ellipsoids were truncated. Shape was characterized by ellipticity of the cavity, E_{cav}, and was calculated as the ratio of the resulting minor and major axis of the inner ellipsoid.
Myofiber orientation in the reference state was quantified by the helix and transverse myofiber angles (90), defined with respect to a local wall coordinate system. This coordinate system consisted of a normalized transmural coordinate, $\overline{\xi}$, a normalized longitudinal coordinate, $\overline{\theta}$, and a circumferential coordinate, ϕ (figure 3.1), as described by Bovendeerd *et al.* (12; 14). The helix angle, α_h, was defined as the angle between the local circumferential direction and the projection of the myofiber direction on the plane normal to the local transmural direction. The transverse angle, α_t, was defined as

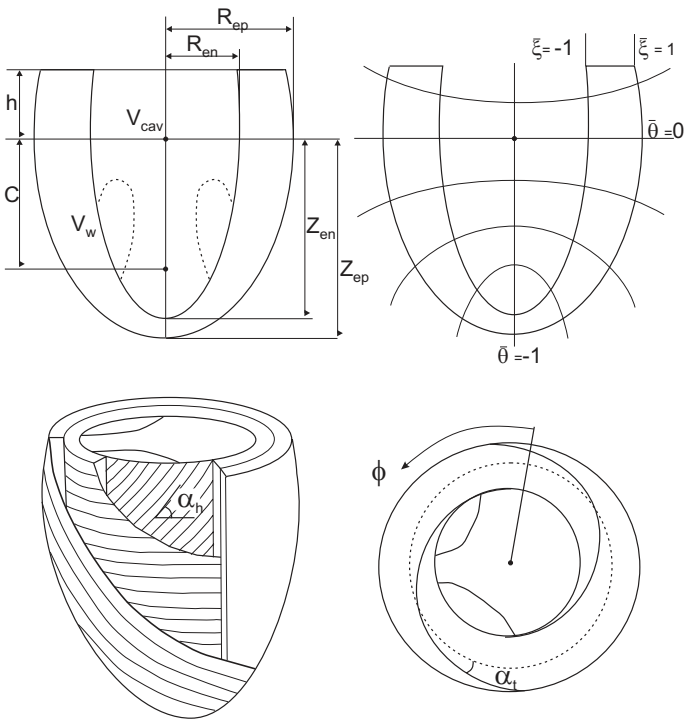

Figure 3.1: *Geometry and myofiber structure of the model of the left ventricle (LV). Upper left: Cross-section through the LV, showing focal length C, truncation height above the equator h, endocardial and epicardial minor ellipsoid axis, R_{en} and R_{ep} respectively, major ellipsoid axes, Z_{en} and Z_{ep}, wall volume V_w and cavity volume V_{cav}. Upper right: Cross-section through the LV showing normalized ellipsoid coordinates $\overline{\xi}$ and $\overline{\theta}$, the dotted lines indicate levels of constant $\overline{\theta}$. Lower left: The helix angle, α_h is shown (Appendix A). Lower right: Top view of the basal plane. The circumferential ellipsoid coordinate, ϕ, and the transverse angle, α_t, are shown (Appendix A).*

the angle between the local circumferential direction and the projection of the myofiber direction on the plane normal to the local long axis direction.
The myocardial tissue was assumed to consist of a connective tissue matrix in which muscle fibers are embedded. Total Cauchy stress in the tissue was the sum of a passive component, $\boldsymbol{\sigma}_p$, and an active component, $\sigma_{\mathbf{a}}$, generated uniaxially in the myofiber direction $\overrightarrow{e_f}$:

$$\boldsymbol{\sigma} = \boldsymbol{\sigma}_p + \sigma_a \overrightarrow{e_f}\overrightarrow{e_f} \tag{3.1}$$

The passive component of the tissue stress was modeled nonlinearly elastic, transversely isotropic, and virtually incompressible, as described by Vendelin

et al. (105). Active stress was uniaxial, depending on myofiber strain, strain rate and time (Appendix A). All myofibers were activated simultaneously. A uniform LV pressure was prescribed at the endocardium, while epicardial load equaled zero. LV pressure and aortic flow were related by aortic hemodynamic impedance, which was simulated by an ideal valve, in series with the aortic input impedance, that was represented by a 3 element Windkessel model (15; 108).
In the calculations, a complete cardiac cycle was simulated according to Bovendeerd *et al* (14). The zero transmural pressure state in diastole was chosen as a reference. The myocardial wall was loaded by ventricular cavity pressure and the active stress generated in the muscle fibers. Stresses and strains in the wall were determined from the equations of conservation of momentum. These equations were converted into a Galerkin-type finite element formulation, elaborated in quadratic 27 node brick elements with three displacement components as nodal degrees of freedom. The left ventricular wall was represented by 108 elements. As a boundary condition, axial motion of all nodes in the basal plane and circumferential motion of four nodes in the endocardial basal ring were suppressed during the cardiac cycle.

3.2.2 Simulations performed

For all geometries, V_w, V_{cav} and truncation height, h were set to 140 ml, 40 ml, and $0.5 \cdot Z_{en}$ respectively (15). By variation of the focal distance C, three different geometries were create: the reference (GeoREF), a more spherical (GeoSPHERE) and a more cylindrical (GeoCYL) geometry (figure 3.2). LV shape was characterized by ellipticity of the cavity, E_{cav}, quantified by the ratio of the minor and major axis of the inner ellipsoid, R_{en}/Z_{en}. The three geometries were characterized by E_{cav} values of 0.35, 0.99 and 0.2 respectively. The choice for the reference geometry was adopted from Bovendeerd *et al* (14). Geometrical parameters are listed in (table 3.1).
In a previous study, myofiber orientation in the reference geometry has been optimized for homogeneous myofiber strain during ejection by Rijcken *et al.* (16; 79). This orientation was used as a reference, FibREF, in this study. Since it yielded a practically homogeneous distribution of myofiber stress in the GeoREF geometry, the analysis of changes in stress distribution due to changes in geometry was facilitated. A brief description of this myofiber orientation distribution is given in Appendix A.
Next we studied the sensitivity of the stress distribution to changes in myofiber orientation in the reference geometry. We varied 1) slope of the transmural

Geometry	:	GeoREF	GeoSPHERE	GeoCYL
C [mm]	:	43.	1.	66.
Shape (E_{cav})	:	0.35	0.99	0.2
h [mm]	:	23.0	11.6	33.7
R_{en} [mm]	:	16.3	23.2	13.5
R_{ep} [mm]	:	31.3	38.8	26.7
Z_{en} [mm]	:	46.0	23.2	67.3
Z_{ep} [mm]	:	53.2	38.8	71.2

Table 3.1: *Geometric parameters of the three evaluated geometries.*

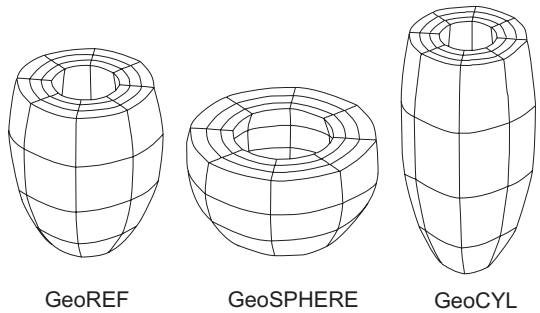

Figure 3.2: *The three evaluated geometries, left: reference geometry, GeoREF, (adopted from Bovendeerd et al. (14)), middle: more spherical geometry, GeoSPHERE, right: more cylindrical shaped geometry, GeoCYL.*

helix angle course, and 2) offset of this course. The slope was varied by multiplication of the helix angle with a factor of 1.1 (Fib*1.1) or 0.9 (Fib*0.9), respectively. These changes correspond to a maximal difference of the helix angle of about 8° compared to the reference myofiber orientation. Offset of the transmural course of the helix angle was changed by +5° (Fib+5), or -5° (Fib-5), respectively. Using these variations, four different myofiber fields were obtained (figure 3.3). The transverse myofiber angle has not been varied.
Using the information on sensitivity of myofiber stress to changes in the distribution of myofiber orientation, the amount of myofiber orientation needed to compensate for geometry variations was estimated.

3.2.3 Presentation of simulation results

In the simulation, the variation of active myofiber stress was calculated as a function of position in the wall and time during the cycle. Active myofiber

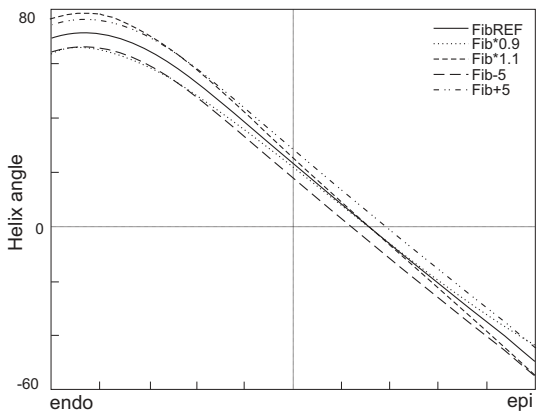

Figure 3.3: *Different choices for the transmural course of the helix angle.*

stress, $T_a(\overline{\xi})$, as averaged over time during the ejection phase was calculated as a function of transmural position, $\overline{\xi}$, in the equatorial slice for all geometries. The transmural distribution of active myofiber stress, $T_a(\overline{\xi})$, was evaluated. Mean, $\overline{T}_a$, and standard deviation of this transmural distribution were also calculated. The inhomogeneity value IH was defined as the ratio of standard deviation and mean value of $T_a(\overline{\xi})$ in percent. Parameter IH indicates homogeneity of the transmural distribution. The inhomogeneity value was also used to evaluate the sensitivity of myofiber stress to variations in myofiber orientation.

3.3 Results

With the reference geometry (GeoREF) and the reference myofiber orientation (FibREF) the transmural distribution of mean myofiber stress during ejection was virtually homogeneous, with calculated inhomogeneity of the stress (IH value) of only 3% (figure 3.4).

Incorporating the default myofiber field (FibREF), into the specific LV geometries (GeoSPHERE, GeoCYL), increased inhomogeneity of the transmural distribution of mean active myofiber stress during ejection. In GeoSPHERE midwall myofiber stress increased at the cost of endo- and epicardial myofiber stress (figure 3.4). In GeoCYL the changes were opposite. The standard deviation to $\overline{T}_a$ increased from 1.5 kPa in the reference geometry, to 5.5 and 5.2 kPa in GeoSPHERE and GeoCYL respectively, which corresponds to an increase of inhomogeneity from 3% in GeoREF, to about 13% in GeoSPHERE and 11% GeoCYL (table 3.2).

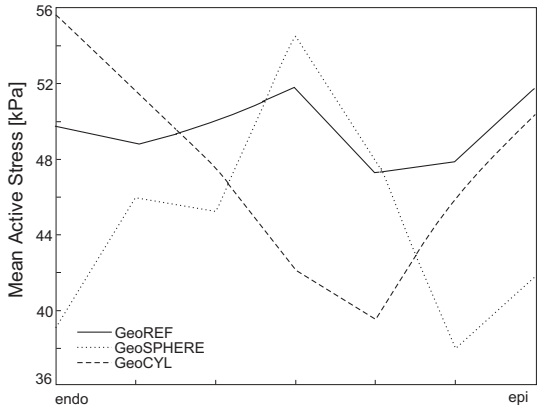

Figure 3.4: *Mean active stress during ejection in the equatorial slice as a function of the transmural position. The reference myofiber orientation, FibREF, was incorporated in the three geometries, GeoREF, the more spherical GeoSPHERE and the more cylindrical GeoCYL.*

$\overline{T}_a \pm sd$ [kPa] (IH [%])		Geometry		
		GeoREF	GeoSPHERE	GeoCYL
Myofiber orientation	FibREF	**48.1±1.5 (3)**	43.2±5.5 (13)	45.9 ± 5.2 (11)
	Fib*1.1	47.4±5.0 (10)	42.7±8.0 (18)	**45.7 ±2.0 (4)**
	Fib*0.9	47.6±4.8 (10)	**43.1±3.6 (8)**	45.0±9.4 (21)
	Fib+5	49.4±5.6 (11)	-	-
	Fib-5	46.2±4.5 (10)	-	-

Table 3.2: *Mean and standard deviation of the mean active stress during ejection, $\overline{T}_a$, for the all geometries, using the reference and changed myofiber orientations. The value between the brackets indicates the inhomogeneity of the stress distribution, IH, quantified by the standard deviation of $\overline{T}_a$ expressed as a percentage of mean stress.*

In GeoREF the effect of incorporating different myofiber distributions was evaluated. With a steeper slope of the transmural course of the helix angle (Fib*1.1) active myofiber stress at the midwall increased. Decrease of the latter slope (Fib*0.9) resulted in opposite effects. Change of the slope of

the helix angle course in GeoREF resulted in an increase of inhomogeneity from 3% with the reference myofiber course (FibREF), to about 10% with the adjusted myofiber courses Fib*1.1 and Fib*0.9. Adding an offset of +5° to the myofiber course resulted in a changed equilibrium between the endo- and epicardial layers. The endocardial stress decreased, whereas the epicardial stress increased. Adding an offset of −5° resulted in opposite effects. Both offset changes induce inhomogeneities on the order of 10 % in the transmural distribution of myofiber stress (figure 3.5, table 3.2).

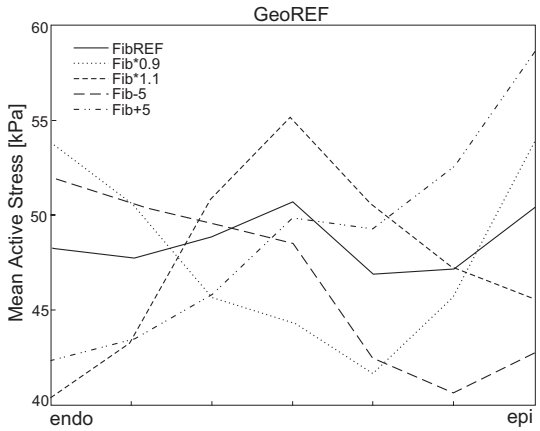

Figure 3.5: *Mean active stress during ejection in the reference geometry (GeoREF), with reference myofiber distribution (FibREF) and four varied myofiber distributions (Fib*0.9, Fib*1.1, Fib-5, Fib+5).*

In the spherical and cylindrical geometries changes in the transmural course of the helix angle lead to similar changes in the transmural stress distribution as observed in the reference geometry (figure 3.6, table 3.2). Consequently, in the spherical geometry a more homogeneous transmural stress distribution was obtained by a shallower helix angle course (Fib*0.9). In the cylindrical geometry, homogeneity of stress was approached with a steeper helix angle course (Fib*1.1).

3.4 Discussion

Although with modern techniques myofiber orientation can be measured *in vitro* with an accuracy of about ±6° (46; 47; 86; 90), *in vivo* measurement is limited to low resolution (78; 99; 100). In a regular heart myofiber orientation

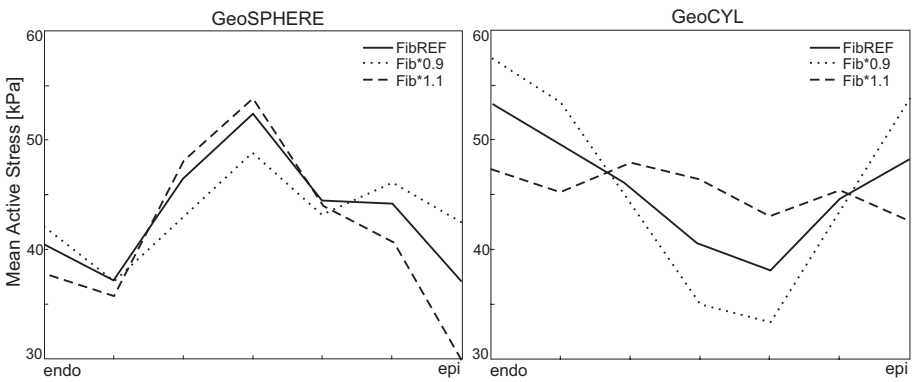

Figure 3.6: *Mean active stress during ejection in GeoSphere (left) and GeoCYL (right), with the reference myofiber distribution (FibREF) and myofiber orientations with variations to the slope of the transmural course of the helix angle (Fib*0.9, Fib*1.1).*

varies about 10°/mm in a direction perpendicular to the wall. Positional resolution of imaging methods for *in vivo* myofiber orientation measurement is expected to be at least a few millimeters, primarily due to motion of the heart. Thus it is to be expected that in patient specific modeling, incorporation of patient specific data on myofiber orientation is not feasible. Therefore the possibility was investigated to use a default myofiber orientation in different geometries, representing a range of individual hearts. Given the major determinants of left ventricular (LV) geometry, the geometry we used in the numerical model was kept as simple as possible.

In healthy subjects, the shape parameter of the left ventricle is typically on the order of E_{cav}=0.35 (90). In patients however, several pathologies have been identified for which left ventricular shape is significantly different from normal. In patients with idiopathic dilated cardiomyopathy for example, left ventricular geometry has been reported to be more spherical, with shape parameter E_{cav} on the order of 0.64 (11). Furthermore, patients with mitral regurgitation have been found to have more spherical chamber geometry both in systole and diastole (37; 107). More cylindrically shaped hearts have been reported in chronic aortic regurgitation (1). If myofiber orientation is obtained from animal experiments, the corresponding geometry may deviate substantially from human cardiac geometry. In the goat for instance, more cylindrically shaped hearts were observed, with shape parameter on the order of E_{cav} = 0.21. In our simulations, we chose to perform large variations in geometry, with E_{cav} ranging from 0.2 to 0.99, to obtain maximal deviations.

Variations in LV geometry are generally accompanied by different wall and cavity volumes when compared to normal. In the present study we chose to maintain these volumes constant, since the mean level of active wall stress is largely determined by the ratio of cavity and wall volume (3). Therefore, this choice allowed us to directly compare myofiber stress distributions between the different geometries.
The effect of incorporating a default myofiber orientation in a specific geometry was evaluated using the distribution of myofiber stress during ejection. This parameter was used because 1) myofiber stress is closely related to local cardiac function, and 2) the mean value of myofiber stress is not sensitive to the used activation sequence (12). Previously (14), myofiber stress was shown to be sensitive to changes in distribution of myofiber orientation.
Reference myofiber orientation (FibREF) was chosen such that for GeoREF myofiber stress was practically homogeneous during ejection, thus facilitating the analysis of occurring changes in the distribution of stress.
Incorporating the default myofiber field (FibREF) into the LV geometries GeoSPHERE and GeoCYL, causes the transmural distribution of mean active myofiber stress to be more inhomogeneous during ejection. This implies that in patient specific modeling, the use of a default distribution of myofiber orientation may induce errors in the calculation of stress. In the biological range of geometries, we expect the related errors in the calculation of the stress distribution to be less than $\pm 10\%$ of the mean stress level.
In the geometry GeoSPHERE homogeneity in stress could be restored by decreasing the slope of the transmural course of the helix angle. Similarly, for GeoCYL an increase of the latter range was needed.
A change in offset of the transmural myofiber orientation affects the transmural mechanical equilibrium. Inhomogeneity in the stress distribution of about $\pm 10\%$ is introduced by a change in offset of $\pm 5°$. Such error is easily introduced in estimating the long axis direction in an experimental situation. Thus, the benefit of accounting for patient specific geometry may be questionable when using experimental data on myofiber orientation.

3.5 Conclusion

The distribution of myofiber stress within the wall of the left ventricle (LV) is sensitive to myofiber orientation and shape of the LV. A default myofiber field which yielded a practically homogeneous distribution of myofiber stress in the reference geometry was incorporated into different geometries. In the more

spherical geometry the calculated midwall myofiber stress decreased relative to the stress in the inner and outer layers. In the cylindrical geometry these changes were opposite. For geometry variations spanning the biological range, changes in active myofiber stress are estimated to be limited to about 10%.
In the reference geometry, changes in myofiber orientation of 10% in slope or a 5° offset led to non-homogeneities in myofiber stress distribution of about 10%. The changes in active stress distribution that were observed as a result of geometry variations, could be compensated by changes in myofiber orientation. For the more spherical and cylindrical geometries, compensation was obtained by a 10% decrease or increase of the slope of the transmural course of the helix angle respectively.
Hence, in patient specific modeling, the use of default values for the myofiber orientation may induce errors in the calculated stress distribution. We estimate these errors to be maximally on the order of 10% of the mean active stress level. A similar change is introduced by a ±5° offset change in myofiber orientation. A ±5° offset error is easily introduced in experimental myofiber orientation data, due to errors in estimating the long axis direction. Thus, the benefit of accounting for patient specific geometry may be questionable when using experimental data on myofiber orientation.

Chapter 4

Myofiber orientation in the infarcted goat heart

L. Geerts, P. Bovendeerd, F. Prinzen, T. van de Nagel,
E. Blezer, K. Nicolay and T. Arts

Numerical studies have shown that the complex myofiber structure of the heart is the main determinant of the distribution of myofiber stress and shortening within the cardiac wall. The sensitivity of local mechanical load to the myofiber orientation makes myofiber re-orientation a potentially powerful adaptive mechanism to restore uniformity of load when local mechanics deviate from normal.
To investigate the hypothesis that cardiac myofiber reorientation serves as a mechanism for cardiac adaptation, in the present study myofiber orientation was assessed quantitatively in hearts in which mechanical load was locally disturbed. This myofiber orientation was then compared to that in normal hearts.
Local mechanical load was disturbed chronically by a transmural infarction in the goat. After 10 weeks of infarction, myofiber orientations were measured post mortem using MR-Diffusion Tensor Imaging (MR-DTI).
In the tissue adjacent to the infarction no significant differences in transmural course of the helix angle were found. Still, the hypothesis that myofiber reorientation serves as a mechanism for cardiac adaptation may not be rejected, since the magnitude of adaptive reorientation may have been below the detection limit.

4.1 Introduction

Cardiac myofiber orientation is highly structured, and remarkably similar across various species (39; 68; 82; 86; 90; 93; 98). Near the equator subepicardial myofibers follow a left handed helix parallel to the outer wall. Near the apex these myofibers cross the wall, then following a right handed helical pathway in the subendocardial layers. Near the base, the myofibers cross over the wall, returning to the subepicardium. At midwall the myofiber orientation is predominantly circumferential.
Numerical studies have shown that this complex structure is the main determinant of the distribution of myofiber stress and shortening within the cardiac wall (5; 14; 22). However, the accuracy with which myofiber orientation has been determined experimentally is insufficient to reliably predict the distribution of stress. In one study (14), for different choices of the myofiber orientation, all within the range of the experimental data, the predicted transmural distribution of equatorial myofiber stress varied from uniformity (60±2 kPa), to severe non-uniformity (40-110 kPa). It has been assumed that cardiac myofiber orientation is designed such that mechanical load is uniform throughout the cardiac wall. This idea is supported by the

work of Peskin (75) who was able to estimate, in a model study, the main characteristics of cardiac myofiber orientation using the assumption of uniform myofiber stress distribution. Rijcken *et al.* (79; 80) optimized myofiber orientation such that myofiber shortening throughout the cardiac wall was distributed uniformly and found the optimum to be within the range of anatomical measurements. Since biological optimization mechanisms generally have a local physiological basis, Arts *et al.* (4) developed a numerical model simulating local adaptation of cardiac myofiber orientation and sarcomere length to local mechanical load. After adaptation myofiber orientation closely agreed with experimental data (4; 82; 90).

The sensitivity of local mechanical load to the myofiber orientation makes myofiber re-orientation a potentially powerful adaptive mechanism to restore uniformity of load when local mechanics deviate from normal. In several studies in which mechanical load was locally disturbed, indications of changes in local myofiber structure have been found. In chronically paced dog hearts, regions of myofiber disarray were observed (2; 56). Also, at the boundaries of a myocardial infarction dispersion of myofiber orientation was reported (88; 109). In these studies however, changes in the spatial distribution of myofiber orientation were not a subject of study.

To investigate the hypothesis that cardiac myofiber reorientation serves as a mechanism for cardiac adaptation, in the present study myofiber orientation was assessed quantitatively in hearts in which mechanical load was locally disturbed. This myofiber orientation was compared to that in normal hearts. Local mechanical load was disturbed chronically by a transmural infarction in the goat. Regional systolic function is known to be impaired in the normally perfused myocardium immediately adjacent to an ischemic region, both in the acute (76; 65) and the chronic phase (58). After 10 weeks of adaptation, myofiber orientations were measured *post mortem* using MR-Diffusion Tensor Imaging (MR-DTI). Myofiber orientations as measured in the regions adjacent to the infarction were compared to those in corresponding regions in healthy controls.

4.2 Methods

Animal handling was performed according to the Dutch Law on Animal Experimentation (WOD) and the European Directive for the Protection of Vertebrate Animals Used for Experimental and Other Scientific Purposes (86/609/EU). The protocol was approved by the Animal Experimental Committee of the University of Maastricht.

4.2.1 Animal Model

In seven female goats, weighing 25 to 50 kg, anesthesia was induced with thiopental 15 mg/kg IV and maintained by ventilation with halothane (1 to 2 %) in a 2:3 mixture of O_2 and N_2. The ECG was recorded from the limb leads. During sterile surgery the thorax was opened and an infarction was induced by ligation of a descending branch of the left circumflex coronary artery (LCx) at the lateral free wall. Ten weeks after infarct induction the animals were anesthetized again. The thorax was re-opened and a clamp was placed around the aorta. The heart was arrested with an injection of 1M KCl into the left ventricular cavity, rapidly excised and rinsed in cold saline. After the removal of the atria the heart was cast in a 20 % gelatin substance in order to maintain shape, and subsequently stored at 4°C. Myofiber orientation was measured within 3 days.
Control measurements were performed on 5 healthy female goats weighing 26-55 kg that were sacrificed for unrelated orthopedic experiments. After an overdose of Euthasate the goats were bled to death. The hearts were excised and the same procedure as for the infarcted hearts was followed.

4.2.2 Myofiber orientation

Myofiber orientation was measured using MR-Diffusion Tensor Imaging (MR-DTI) (7; 47; 86). ^1H MR-DTI measurements were performed according to the protocol described in chapter 2. As a result myofiber orientation was known with respect to the magnet coordinate system in adjoining slices of 3 mm thick at a resolution of 0.78×0.78 mm^2.
The reliability of the calculated primary eigenvector was assessed by the degree of anisotropy of the diffusion tensor, as quantified by the ratio between both largest eigenvalues.
To quantify myofiber orientation, a local wall-bound coordinate system of the heart was defined relative to the global magnet coordinate system. A best fit circle through the pixels containing circumferentially oriented midwall myofibers yielded the center of the left ventricle (LV) in each slice. The local long axis direction pointing to the base was then determined as the best fit line through the thus determined centers in 5 adjoining slices. In each slice, the related LV center served as the origin of a local cylindrical coordinate system. The $\Phi = 0$ reference of the coordinate system was defined along the anterior right ventricular (RV) fusion site.
The helix angle component of myofiber orientation, α_h, was defined as the

angle between the myofiber direction and the plane perpendicular to the local long axis direction. In each slice, the LV wall was divided into 36 adjoining sectors, each being 10° wide. The helix angle was determined as a function of the radius for all pixels within each sector. This function was fitted with a 5th order polynomial. The radius $R_0(\Phi)$, at which the helix angle changes sign was determined for each sector and used to convert the transmural position, R, to a normalized transmural position, h:

$$h = \frac{R - R_0}{R_0} \tag{4.1}$$

The transmural course of the helix angle was characterized by its slope. For all sectors in each heart this slope was determined by linear fit of the helix angle versus the normalized radius h for the compact portion of the wall, defined by $h >$-0.3.

4.2.3 Infarct localization

Infarctions were localized on the basis of local wall thickness. To determine wall thickness, the contours of the LV wall were determined visually in the MR images. Again, in each slice the LV wall was divided in 36 sectors, each being 10° wide. For each sector the total number of pixels in both the LV cavity and LV wall was determined. From this number the outer radius was calculated. The number of LV wall pixels was then used to determine wall thickness (WT). Mean and standard deviation of wall thickness were determined in at least 100 sectors remote from the infarct location. The infarction was localized as the area in which wall thickness was less than mean wall thickness minus 4 times the standard deviation.

Infarct size was expressed as the percentage of midwall surface affected. To this end in each slice midwall radius, R_{mw}, was calculated as the average R_0. The number of sectors in which infarct tissue was present yielded the affected angle, ϕ_{aff}, for each slice. The affected midwall surface for one slice could thus be calculated as $R_{mw} \cdot \phi_{aff} \cdot th_{slice}$, where th_{slice} is the slice thickness in base to apex direction. The total affected midwall surface was obtained by summation over all slices.

For comparison, magnetic resonance T_2 relaxation times and cardiac perfusion as measured with the microsphere method were assessed as well. In order to determine MR T_2 times, images were acquired in a spin-echo MRI sequence using echo times (TE) of 10, 30, 55, 80 and 110 ms. Repetition time TR was 4 seconds. T_2 values were then calculated from signal attenuation. T_2 values

were evaluated in the same sectors as selected for determination of LV wall thickness.
Cardiac perfusion measurements were performed using fluorescent microspheres with a diameter of 15 μm. Microspheres were injected through a catheter in the LV chamber before and 3-6 weeks after infarct induction. Each injection contained $3{\cdot}10^6$ microspheres, labelled with blue, blue-green, yellow-green, orange, red or crimson fluorescent labels (Molecular Probes, Eugene, OR). After the *post mortem* MRI measurements had been completed, two 1 cm thick short axis slices were selected. One of these slices contained the mid-infarct region, the other slice was just basal to the infarction. The slices were cut into 8 sectors. One sector contained the mid-infarct region, while on each side of the infarct region three sectors of about 30° wide were selected. The remaining sector contained the septum. Microspheres were isolated from the myocardial samples by tissue digestion and centrifugal sedimentation. Consecutively, fluorescence was determined by use of fluorimetry (103). Relative perfusion values were obtained, using measurements in the septum as a reference.

4.2.4 Comparison of myofiber orientation in normal and infarcted hearts

Throughout the infarcted hearts, the transmural course of the helix angle was characterized by the slope of this course. In addition, a more detailed analysis was performed in 3 areas, A, P and B, selected as indicated in figure 4.1. The location of these areas was chosen as follows. The apex-to-base length of the infarction was determined from the number of short-axis slices in which infarcted tissue was detected to be present. In the slice at mid-infarct position, areas A and P were chosen as a 10° wide sector adjacent to the infarction in anterior and posterior direction respectively. In the slice just basal to the infarction area B was chosen as a 10° wide sector as near as possible to the infarction. Since infarct size and location may vary, corresponding sectors in the control hearts were selected for each infarcted heart separately on the basis of anatomical landmarks that were visible in the MR images.
To calculate the average transmural course of the helix angle for control hearts in a particular sector, the helix angle distributions of the five control hearts were grouped per sector. Helix angle was related to the normalized radius by a 5th order polynomial fit over all pixels of the five sectors. In addition, the 95 % prediction limit was calculated.
The transmural course of the helix angle in sectors of infarct hearts was

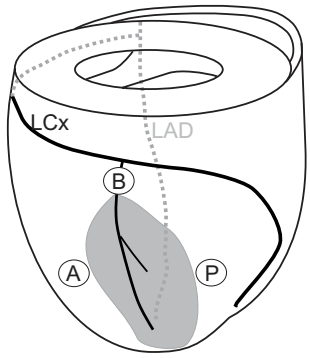

Figure 4.1: *Regions selected for detailed analysis of the transmural course of the helix angle. A: Anterior with respect to the infarction, P: Posterior with respect to the infarction, B: Basal to infarction. LCx: Left circumflex coronary artery, LAD: Left anterior descending coronary artery.*

compared to this course in corresponding sectors of the control hearts. If the helix angle course of the infarct hearts fell outside the 95 % prediction limit as calculated for the control hearts, the myofiber orientation was considered significantly different.

4.3 Results

Results are presented for the three goats in which a transmural infarction was properly induced. Two goats died due to the infarction, and in two goats the infarction appeared not to be transmural, since no marked wall thinning was observed in the MR images.

Infarctions were located on the basis of wall thickness. An example of a wall thickness map for heart G0228 is shown in the upper left panel of figure 4.2. The infarct area is recognized by its relatively thin wall. In this heart, infarct size was 6.9% of the total midwall surface. Although infarct size and location varied, all infarctions were located below the equator at the lateral side of the heart. Infarcted tissue was found in at least 3 slices, which corresponds to a minimal apex-to-base length of the infarction of 1 cm. Infarct size in both other hearts was 2.4 and 18.6% of total midwall surface.

MR T_2 values were found to be elevated in the infarction in all hearts. In the tissue remote from the infarction, average T_2 was 42.4 $\pm$ 1.2 ms, whereas in the infarct region T_2 averaged 105.5 $\pm$ 9.4 ms. The T_2 map for heart G0228 is shown in the lower right panel of figure 4.2. The area of elevated T_2 coincided closely with the area where the wall was thinner.

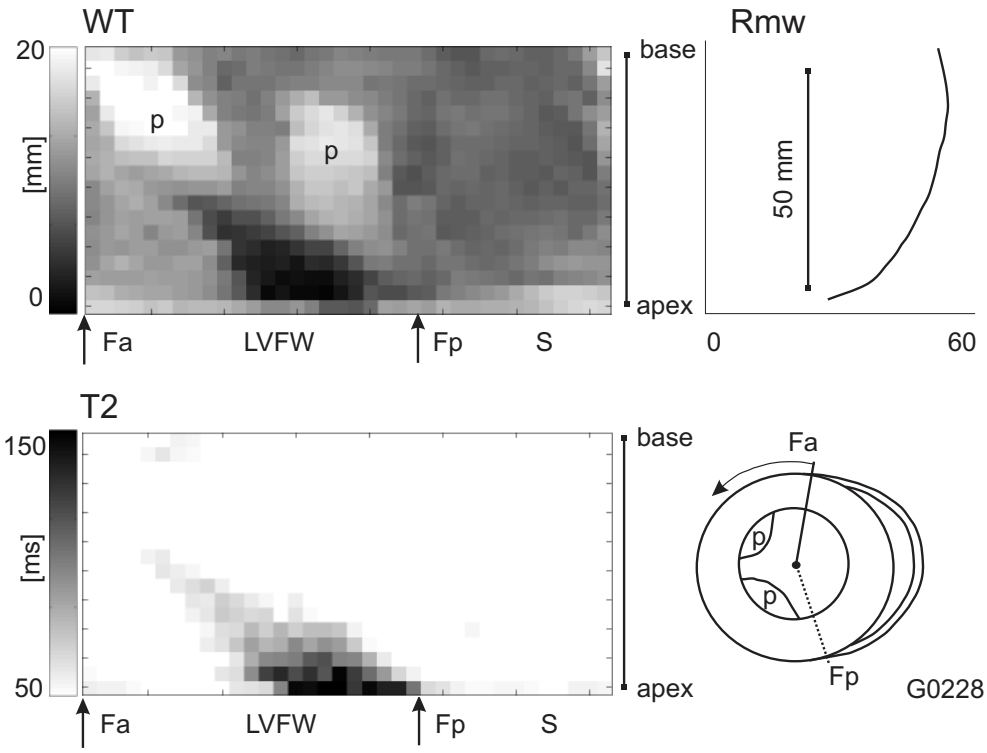

Figure 4.2: *Heart G0228. Upper left: Wall thickness map, the infarction is recognized by its low wall thickness, which corresponds to the dark areas. The bright areas indicate the papillary muscles. Upper Right: Mean midwall radius, R_{mw}, as a function of the apex to base position. Lower left: MR T_2 map, T_2 values within the infarct region are elevated (dark area). Lower right: Illustration of orientation of the maps, Fa: Anterior fusion site of LV and RV walls, Fp: Posterior fusion site of LV and RV walls, p: papillary muscles.*

Within the infarct region, myocardial blood flow was decreased by 39±11% when compared to blood flow in the remote region. The blood flow was compared to the local wall thickness data as shown for heart G0228 in figure 4.3.

The mean ratio of λ_1 over λ_2, the two largest eigenvalues of the diffusion tensor, was 1.87 ± 0.05 remote from the infarction. Within the infarct region this ratio dropped to 1.23 ± 0.03. Adjacent to the infarct region no significant changes in the ratio of λ_1 over λ_2 were observed (figure 4.4).

Remote from the infarction in the lateral free wall, the slope of the transmural helix angle course averaged -118.9 $^\circ \pm 29^\circ$. Outside the infarct region no

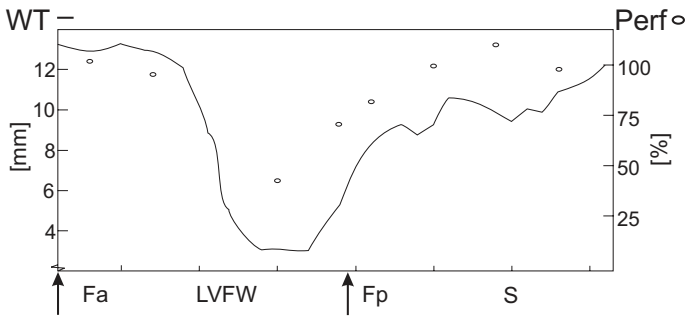

Figure 4.3: *Comparison of local wall thickness (-) and cardiac perfusion (o) 6 weeks after infarct induction for a slice of heart G0228 containing the mid-infarct region. Within the infarct region, perfusion was circa 50% of normal septal values.*

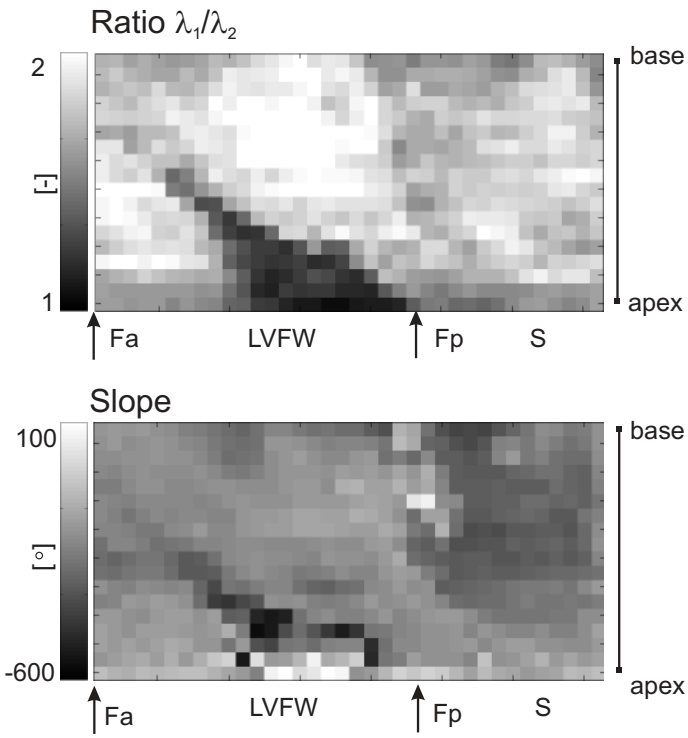

Figure 4.4: *Same heart as in figure 4.2 (G0228). Upper panel: Ratio between the two largest eigenvalues. Within the infarct region this ratio is markedly decreased (dark area). Lower panel: Slope of the transmural course of the helix angle. Within the infarct region the slope seems more variable.*

deviations in the slope of the helix angle as compared to normal hearts were observed. In infarct tissue, the slope was more variable (figure 4.4).
The transmural course of the helix angle in the selected regions adjacent to the infarction is shown in figure 4.5 for all infarcted hearts. The region between the solid lines indicates the 95% prediction limit of the transmural course of the helix angle for corresponding regions in normal hearts. The transmural course of the helix angle in normal and in infarcted hearts was not significantly different.

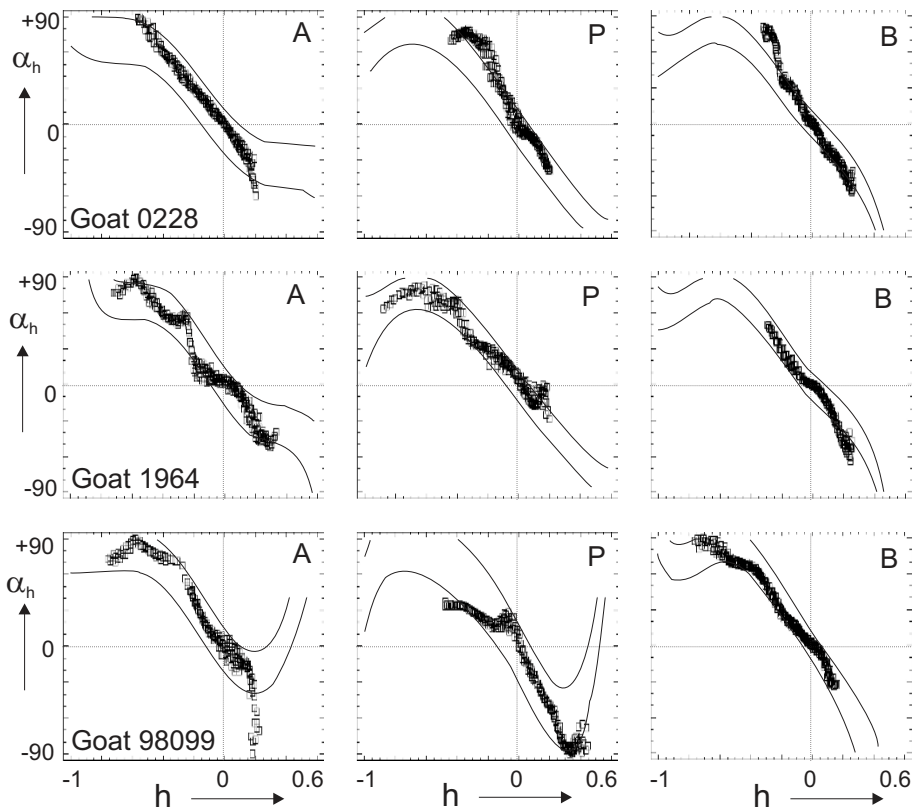

Figure 4.5: *Transmural course of the helix angle for the regions as specified in figure 4.1. The squares indicate the helix angle, α_h, as a function of the normalized radius, h, in the infarct hearts. The solid lines indicate the 95% prediction limits for the transmural course of the helix angle in corresponding regions in normal hearts. Note that the 95% prediction limits are different for the three hearts, due to variations in infarct size and location.*

4.4 Discussion

In the present study changes in cardiac myofiber orientation were determined in response to a small chronic transmural infarction. The infarctions had to be relatively small ($< 20\%$ of LV midwall affected surface) in order to prevent cardiac failure.
The goat was chosen because its heart is large enough to allow measurement of myofiber orientation with sufficient spatial accuracy. Moreover, in the goat heart the number of coronary artery collaterals is limited, thus facilitating the induction of a transmural infarction by simple ligation of a coronary artery (17; 62). Furthermore in the goat heart the Purkinje system is well developed, which diminishes the risk of arrhythmia due to infarction.
The animal was sacrificed 10 weeks after infarct induction to allow changes in cardiac tissue structures to develop. Since in the infarct region scar tissue forms mainly during the first 6 weeks (55), the surrounding tissue was allowed to adjust to the new situation over a period of 4 weeks. It is unknown whether a steady state situation is present at the moment of sacrifice, since the time needed for the various adaptive processes in the heart remains largely unknown. However, polarized light studies by Whittaker *et al.* (109) indicate myofiber disarray in the cardiac muscle cells adjacent to the infarction as early as one week after infarct induction.
Infarct localization was performed on the basis of wall thickness distribution (55; 67). The result agreed with the measured myocardial perfusion. The spatial resolution of the perfusion measurements however, was too limited to serve as a basis for infarct localization. It should also be noted, that in the infarct region, where wall thickness drops to about 3 mm, myocardial perfusion is still up to 50% of perfusion in the septum remote from the infarct location. This may be due to intrusion of normally perfused tissue into the infarct region. Recent studies have also indicated that vascularization remains present in the infarct scar up to at least 8 weeks post infarction (94).
Within the infarct region, magnetic resonance MR T_2 relaxation times appeared to be significantly elevated. This finding corresponds to observations by Hsu *et al* in formalin fixed hearts (48), although the process responsible for *post mortem* T_2 elevation is not yet understood. The spatial distribution of T_2 times correlated well to local wall thickness, which indicates that *post mortem* MR T_2 values may be used for infarct localization. Care should however be taken, since it is not clear how T_2 values change in case of stunning or hibernating myocardium.
Myofiber orientation was measured using MR Diffusion Tensor Imaging at

a resolution of 1.8 mm^3. This resolution was sufficient to allow for local characterization of the transmural distribution of myofiber orientation. The ratio between the largest (λ_1) and the second (λ_2) eigenvalue is an indicator of how well the direction of largest diffusivity, and hence myofiber orientation, was determined within a voxel. Outside the infarct region a decrease of the ratio of λ_1 over λ_2 may be ascribed to disarray occurring at voxel level.
Within the infarct region the λ_1 over λ_2 ratio decreases. Histological and ultrasonic studies of infarct scar collagen organization indicate that a highly ordered arrangement of scar collagen fibers exists (109; 110). Apparently, this fiber organization can not be accurately detected using MR-DTI.
In the region adjacent to the infarction, myofiber disarray was reported by Whittaker (109). In the same region in our study however, the ratio of λ_1 over λ_2 remained largely normal. Therefore we expect myofiber disarray to be limited.
It was not possible to measure myofiber orientation before and after the infarction in the same hearts, since the *in vivo* application of MR-DTI is so far limited to a low spatial resolution and a small number of tissue slices (78). Therefore, myofiber orientation as measured in infarcted hearts was compared to that in a healthy control group.
The slope of the transmural course of the helix angle was selected to characterize the spatial distribution of the myofiber orientation throughout the heart. No significant changes in the slope of the helix angle were observed in the region adjacent to the infarction.
The radius at which the helix myofiber angle equals zero, R_0 was used as a reference radius to which all transmural distances were normalized in this study. R_0 is much better defined than the more commonly used endocardial wall and has a smooth appearance.
To the best of the authors' knowledge the present study is the first one in which myofiber orientation in the region adjacent to an infarction has been evaluated quantitatively. Previously, morphological (10; 30; 31) and structural (38; 109) changes at the microscopic level were reported in the tissue around a transmural infarction. The effect of these changes on the spatial distribution of the myofiber orientation, was not reported. We found no significant changes in the spatial distribution of myofiber orientation around a transmural infarction.
We expected to find changes in myofiber orientation, based upon the hypothesis that myofiber orientation adapts to the changed mechanical load in the region around the infarction. The fact that no changes were observed may be due to several causes. First of all, the mechanical load in the borderzone of the infarction may not have changed, which implies that no stimulus

for adaptation existed. Although mechanical load in the borderzone of the infarction was not measured in this study, it was reported to change both in experiments (58) and numerical studies (13). Secondly, cardiac myofibers may not be able to adapt their orientation. However, in several studies regarding cardiac pacing, myocardial disarray, which can be regarded as an ill conditioned adaptive process, was reported to develop (2; 56; 57). Also around a chronic infarction, disarray was observed (63; 109). Furthermore, Tezuka *et al.* measured changes in the distribution of myofiber orientation in response to changed loading conditions in pig hearts (97). These results indicate that myofiber reorientation may be possible. Finally, adaptive changes in myofiber orientation may have been too small to detect. It has been shown that local mechanical load is very sensitive to myofiber orientation. Small variations in the myofiber orientation, within the range of the measuring accuracy ($\pm 10°$), resulted in large variations ($\pm 50\%$) of calculated myofiber stress (14).

4.5 Conclusion

To investigate the hypothesis that cardiac myofiber reorientation serves as a mechanism for cardiac adaptation, in the present study myofiber orientation was assessed quantitatively in hearts in which mechanical load was locally disturbed.

Infarct localization was based on local wall thinning, but it was found that MR-T_2 values and diffusion anisotropy could serve as a basis of infarct localization as well.

In the tissue adjacent to the infarction no significant differences in transmural course of the helix angle were detected. Still, the hypothesis that myofiber reorientation serves as a mechanism for cardiac adaptation may not be rejected, since the magnitude of adaptive reorientation may have been below the detection limit.

Chapter 5

Myofiber orientation in the infarct borderzone – a model study

L. Geerts, R. Kerckhoffs, P. Bovendeerd and T. Arts

The presence of a cardiac infarction alters local mechanical load in the cardiac wall. The myocardial tissue may adapt to changing loading conditions, possibly to restore homogeneity of mechanical load in the healthy tissue. The sensitivity of local mechanical load to myofiber orientation makes myofiber reorientation a potentially powerful adaptive mechanism to restore homogeneity of load. The purpose of this study was to estimate quantitatively the adaptation of myofiber orientation needed to restore homogeneity of mechanical load in the normally perfused borderzone region adjacent to a chronic transmural infarction.
In a simulation of the mechanics of the infarcted left ventricle the inhomogeneity of transmural distribution of active myofiber stress in the borderzone adjacent to the infarction increased from 5 to 15%. Inhomogeneity of active myofiber stress in the borderzone could be compensated by a transmural rigid body rotation on the order of 10° of the myofibers in the wall in patches near the infarct.
We conclude that myofiber reorientation may serve as an adaptive mechanism to restore homogeneity of mechanical load in the borderzone of a transmural myocardial infarct. This reorientation remains however below the level of detection for most measuring methods of myofiber orientation.

5.1 Introduction

The presence of a cardiac infarction alters mechanical load in the cardiac wall. Global pump function is compromised, primarily due to the loss of contractile function in the ischemic zone. A secondary loss originates from the work that is converted into elastic energy in stretching the ischemic zone during systole. In addition, local systolic function is known to be impaired in the myocardium adjacent to an ischemic region, even though perfusion is normal. In the acute phase, circumferential shortening decreases and shear strains increase (13; 64; 65; 76). In the chronic phase, the stiff infarction tethers the adjacent tissue, resulting in a decrease of systolic myofiber shortening (58).
There are indications that the heart adapts to the changed loading conditions in the presence of an infarction, possibly to restore homogeneity of loading conditions in the remaining healthy tissue. Hypertrophic growth has been reported to occur in the normally perfused myofibers of an infarcted heart (26).
Indications of adaptive changes in local myofiber structure have been found at the boundaries of a myocardial infarction. These changes comprise structural

changes (30; 31; 73), changes in cell-cell contact and cell-extracellular matrix contact (63), and dispersion of myofiber orientation (66; 88; 109).
However, detailed measurement of myofiber orientation with MR-DTI in a region adjacent to a 10 weeks old infarction, showed that this orientation was not significantly different from normal (Chapter 4). This might mean that myofibers did not reorient indeed. However, it may also be that myofibers did adapt their orientation to even out differences in mechanical load effectively, but that the changes in myofiber orientation were below the level of measuring accuracy ($\pm 6°$). This possibility is coherent with the finding that, in the normal heart, mechanical load is very sensitive to changes in myofiber orientation (14; 80).
Therefore, the purpose of this study was to estimate quantitatively adaptation of myofiber orientation needed to restore homogeneity of mechanical load in the normally perfused region adjacent to a chronic transmural infarction. We define this region here as borderzone region. Cardiac mechanics near an infarction was simulated in a numerical model. The infarction was modelled as a non-contractile, stiff region. Around the infarction a borderzone region was defined, in which myofiber orientation could be varied. In this region the sensitivity of the distribution of active myofiber stress to local changes in myofiber orientation was evaluated. Finally, the amount of myofiber reorientation needed to restore homogeneity of mechanical load, was estimated.

5.2 Methods

5.2.1 Description of the model

The model used for the numerical simulations has been described in detail elsewhere (13; 14; 105). Briefly, the left ventricular (LV) geometry was approximated by truncated confocal ellipsoids representing inner and outer wall surfaces. Myofiber orientation in the reference state was quantified by the helix and transverse myofiber angles (90), defined with respect to a local wall coordinate system (figure 5.1). Along the axes of this coordinate system a normalized transmural coordinate, $\overline{\xi}$, a normalized longitudinal coordinate, $\overline{\theta}$, and a circumferential coordinate, ϕ, were defined (14). The helix angle, α_h, was defined as the angle between the local circumferential direction and the projection of the myofiber direction on the plane normal to the local transmural direction. The transverse angle, α_t, was defined as the angle between the local circumferential direction and the projection of the myofiber direction on the plane normal to the local long axis direction.

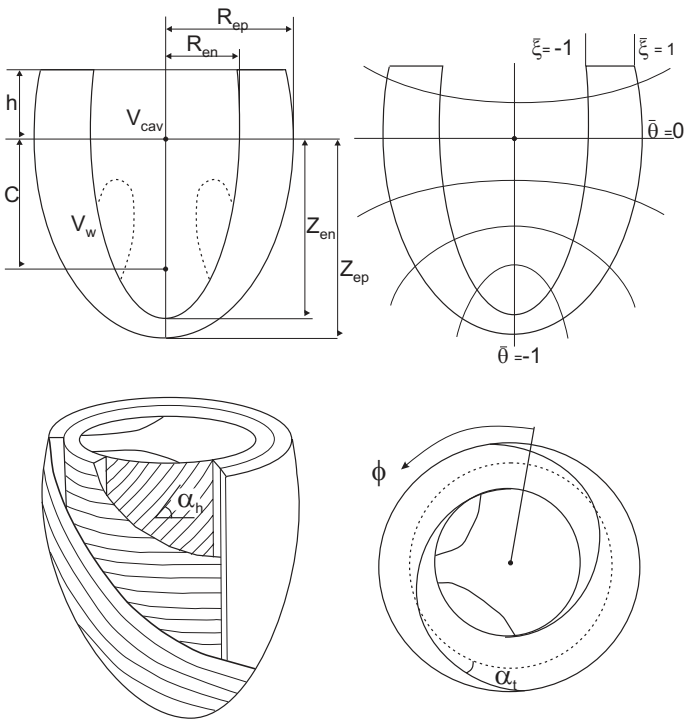

Figure 5.1: *Geometry and myofiber structure of the model of the left ventricle (LV). Upper left: Cross-section through the LV, showing focal length C, truncation height above the equator h, endocardial and epicardial minor ellipsoid axis, R_{en} and R_{ep}, and major ellipsoid axes, Z_{en} and Z_{ep} respectively. Wall and cavity volume are indicated by V_w and V_{cav} respectively. Upper right: Cross-section through the LV showing normalized ellipsoid coordinates $\overline{\xi}$ and $\overline{\theta}$, with dotted lines indicating levels of constant $\overline{\theta}$. Lower left: Illustration of the helix angle, α_h (Appendix A). Lower right: Top view of the basal plane. The circumferential ellipsoid coordinate, ϕ, and the transverse angle, α_t, are shown (Appendix A).*

The myocardial tissue was assumed to consist of a passive connective tissue matrix in which active myofibers were embedded. Total Cauchy stress in the tissue was the sum of a passive component, $\boldsymbol{\sigma}_p$, and an active component, $\sigma_{\mathbf{a}}$, generated uniaxially in the myofiber direction $\overrightarrow{e_f}$:

$$\boldsymbol{\sigma} = \boldsymbol{\sigma}_p + \sigma_a \overrightarrow{e_f}\overrightarrow{e_f} \tag{5.1}$$

The passive component of the tissue stress was modelled nonlinearly elastic, transversely isotropic, and virtually incompressible, as described by Vendelin *et al.* (105). Active stress was uniaxial, depending on myofiber strain,

strain rate and time. LV pressure was prescribed to be uniform at the endocardium, while epicardial pressure was set to zero. All myofibers were activated simultaneously. During ejection, the aortic hemodynamic load was simulated by an ideal valve, followed by the aortic input impedance, which was simulated by a 3 element Windkessel model (15; 108).
A chronic transmural infarction was modelled as a region having no active stress component σ_a. Passive stiffness in the infarction was modelled to be 5 times higher than in the normal tissue (43; 72). The size and location of the infarcted region, Γ_{inf}, were defined relative to the local wall coordinate system (figure 5.2):

$$\mathbf{x}(\phi, \overline{\theta}, \overline{\xi}) \in \Gamma_{inf} \quad \text{if} \quad \begin{cases} \frac{\pi}{3}(\overline{\theta} + \frac{1}{4}) \leq \phi \leq -\frac{\pi}{3}(\overline{\theta} + \frac{1}{4}) \\ \overline{\theta} \leq -\frac{1}{4} \\ -1.0 \leq \overline{\xi} \leq +1.0 \end{cases} \tag{5.2}$$

A borderzone surrounding the infarction, Γ_{bz}, was defined as:

$$\mathbf{x}(\phi, \overline{\theta}, \overline{\xi}) \in \Gamma_{bz} \quad \text{if} \quad \ni \Gamma_{inf} \quad \text{and} \begin{cases} \frac{\pi}{2}\overline{\theta} \leq \phi \leq -\frac{\pi}{2}\overline{\theta} \\ \overline{\theta} \leq 0.0 \\ -1.0 \leq \overline{\xi} \leq +1.0 \end{cases} \tag{5.3}$$

In the latter region, myofiber orientation was varied, while material properties were maintained.

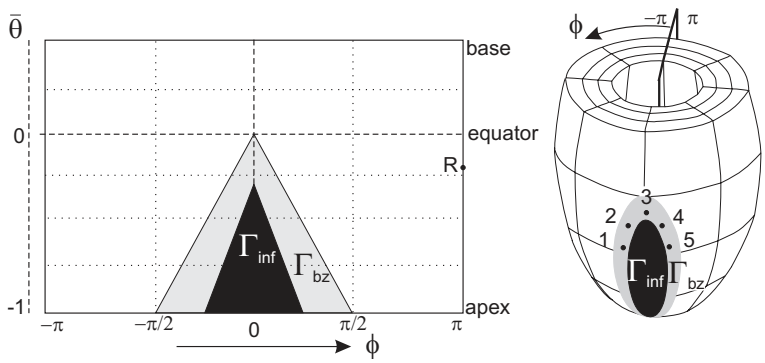

Figure 5.2: *Infarcted region (black area), Γ_{inf}, and borderzone region, Γ_{bz} (gray area). The locations that were used for analysis are indicated (•). Locations 1 to 5 are located in the borderzone, location R is located remote from the infarction opposite to location 3. In transmural direction the infarction extends from the endocardial to the epicardial surface.*

In the calculations, a complete cardiac cycle was simulated according to Bovendeerd *et al* (14). The initial zero LV pressure state was chosen as a reference. The myocardial wall was loaded by LV cavity pressure and the active stress generated in the muscle myofibers. Resulting stresses and strains in the wall were determined from the equations of conservation of momentum. These equations were converted into a Galerkin-type finite element formulation, elaborated in quadratic 27 node brick elements with three displacement components as nodal degrees of freedom. The geometry of the left ventricle was represented by 108 elements. During the cardiac cycle, axial motion of the basal plane and circumferential motion the endocardial basal ring were set to zero.

5.2.2 Simulations performed

In a previous study, myofiber orientation has been optimized for homogeneous myofiber strain during ejection by Rijcken *et al.* (16; 79). This myofiber course was used as reference distribution of myofiber orientation (FibREF) because the resulting distribution of myofiber stress obtained in a healthy heart was practically homogeneous. Thus the analysis of changes in stress distribution due to the presence of an infarction was facilitated. A brief description of this myofiber orientation distribution is given in Appendix A.
We studied the sensitivity of the stress distribution to local changes in myofiber orientation in the borderzone, Γ_{bz}. We locally varied 1) slope of the transmural helix angle course, and 2) offset of this course. The slope was varied by multiplication of the helix angle with a factor of 1.1 (Fib*1.1) or 0.9 (Fib*0.9), respectively. These changes correspond to a maximum difference of the helix angle of about 8° as compared to the reference. Offset of the transmural course of the helix angle was changed by +10° (Fib+10), or -10° (Fib-10), respectively. The transverse myofiber angle has not been varied. Using these variations, four different myofiber fields were obtained (figure 5.3).
Using the information on sensitivity of local myofiber stress to local changes in the distribution of myofiber orientation, an estimate was made of myofiber reorientation needed to restore an homogeneous stress distribution.

5.2.3 Presentation of simulation results

The results of the simulations were evaluated at 5 locations surrounding the infarcted region, and at a location remote from the infarction, opposite to the location 3, as indicated in figure 5.2.

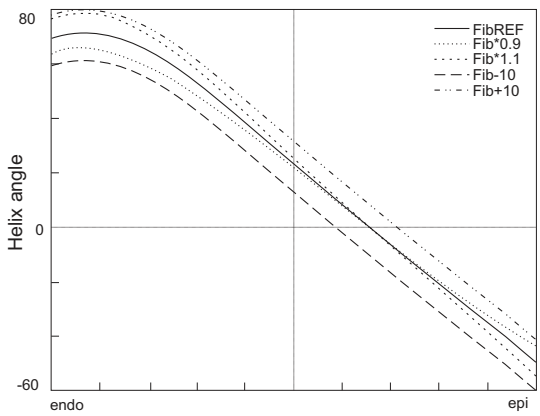

Figure 5.3: *Different choices for the transmural course of the helix angle in the borderzone.*

In the simulation, the variation of active myofiber stress was calculated as a function of position in the wall and time during the cycle. Active myofiber stress, $T_a(\overline{\xi})$, as averaged over time during the ejection phase was calculated as a function of transmural position, $\overline{\xi}$. Mean, $\overline{T}_a$, and standard deviation of this transmural distribution were also calculated. The distribution of myofiber stress around the infarction was evaluated by comparing $\overline{T}_a$ at the 5 locations. An inhomogeneity parameter IH, indicating homogeneity of the transmural distribution, was defined as the ratio of standard deviation and mean value of $T_a(\overline{\xi})$ in percent. This parameter was also used to evaluate the sensitivity of myofiber stress to variations in myofiber orientation.

5.3 Results

Remote from the infarcted region (location R in figure 5.2), active myofiber stress was practically homogeneous. Mean myofiber stress during ejection averaged 44.6±2.4 kPa, which corresponds to an inhomogeneity value (IH) of about 5%. Transmural active myofiber stress in the borderzone was more inhomogeneous as compared to the remote location (figure 5.4).
For locations 1 and 2, mean active myofiber stress during ejection is low in the epicardial layers, whereas in the endocardial layers high active stresses occur. At the other side of the infarct region, in locations 4 and 5, opposite effects are visible. In location 3, which is basal to the infarcted region, midmyocardial myofiber stress is lower than at the endo- and epicardial layers.
Mean active myofiber stress at the locations surrounding the infarct region is

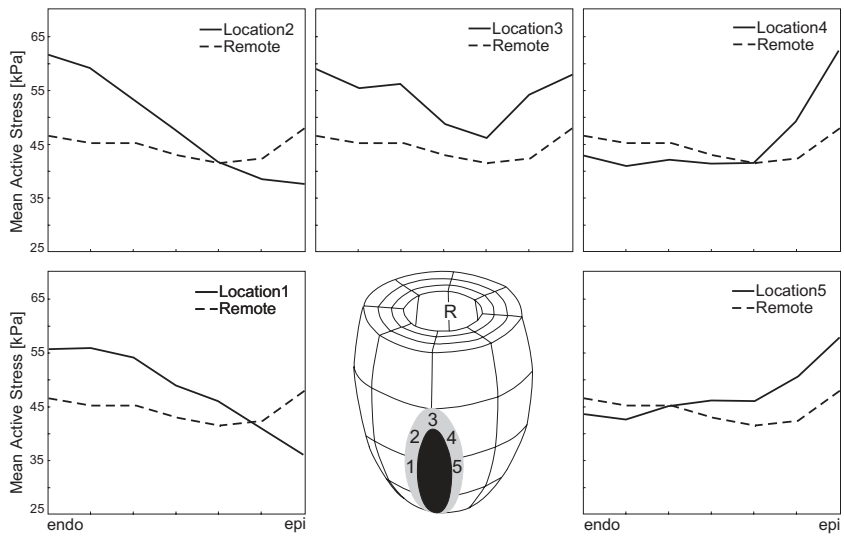

Figure 5.4: *Transmural distribution of active myofiber stress, averaged over the ejection phase for locations 1 to 5 surrounding the infarction. These locations are indicated in the figure. For comparison, the distribution of myofiber stress in the remote region is shown by the dashed line.*

comparable to normal active myofiber stress, except for location 3, where stress is significantly elevated. At all locations surrounding the infarcted region, inhomogeneity values were significantly higher than in the remote location, ranging from 9% to 20% (table 5.1).

The influence of local variations in the distribution of myofiber orientation is shown in figure 5.5. For locations 1 and 2, out of the four variations, the negative offset variation, indicating a counterclockwise rotation of all myofibers in that region as observed from the outside, yielded the most homogeneous transmural distribution of active myofiber stress. In location 1, addition of this offset decreased inhomogeneity (IH) from 20% to 11%, in location 2 IH dropped from 15% to 10%. For locations 4 and 5, the transmural distribution of active myofiber stress was made more homogeneous by increasing the offset by $+10°$, with decreasing IH values from 17% to 13% and from 11% to 4% respectively. For location 3 a slight improvement of homogeneity could be reached when the slope of the transmural course of the helix angle was decreased by 10%. In this case IH values decreased from 9% at normal myofiber orientation to 7% at locally adjusted myofiber orientation. At location 3, mean active myofiber stress during ejection, $\overline{T}_a$, could be reverted to normal values by increasing the offset by $+10°$.

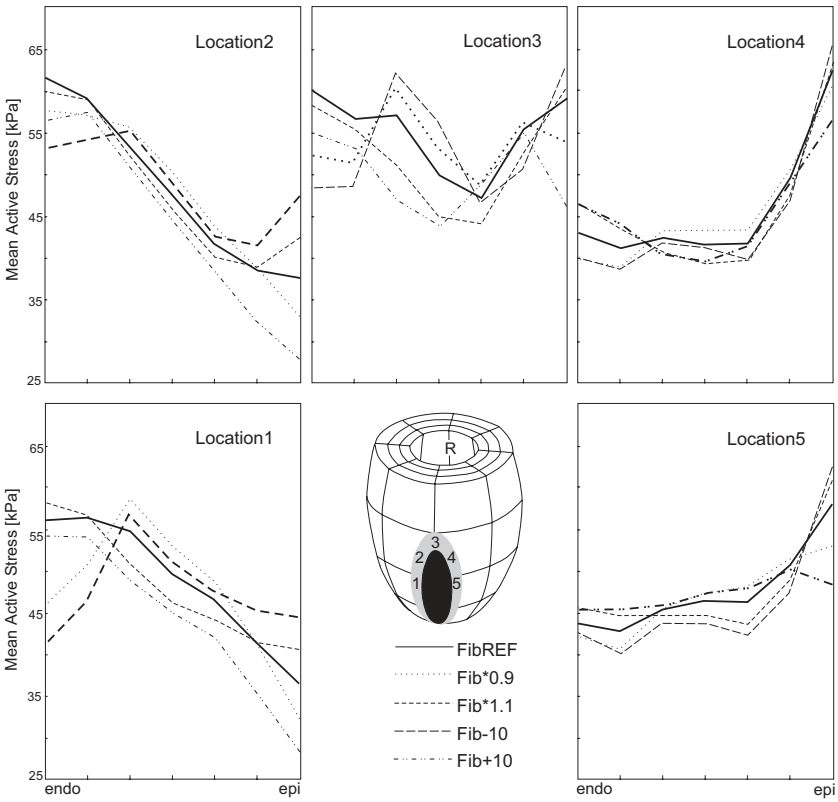

Figure 5.5: *Transmural distribution of active myofiber stress, averaged over the ejection, for locationss 1 to 5 surrounding the infarction for different distributions of local myofiber orientation (Ref, Fib*0.9, Fib*1.1, Fib-10 and Fib+10). Reference myofiber orientation (Ref) and myofiber orientation which resulted in minimum inhomogeneity are printed in bold. The locations are indicated in the figure.*

$T_a \pm sd$ [kPa] (IH [%])		Location					
		1	2	3	4	5	Remote
Myofiber orientation in Γ_{bz}	REF	48.7±7.7 (15)	48.8±9.8 (20)	54.3±4.7 (9)	45.8±7.9 (17)	47.7±5.2 (11)	44.6±2.4 (5)
	Fib*1.1	48.0±7.1 (15)	48.2±8.7 (18)	52.7±6.2 (11)	46.0±8.5 (19)	47.7±6.1 (13)	44.1±1.9 (4)
	Fib*0.9	47.2±8.6 (18)	47.8±9.7 (20)	**53.6±3.7 (7)**	45.3±7.6 (17)	47.4±4.5 (9)	44.7±2.8 (6)
	Fib+10	44.1±9.7 (22)	43.6±11.6 (27)	49.8±4.6 (9)	**45.1±5.9 (13)**	**47.0±1.8 (4)**	44.5±2.7 (6)
	Fib-10	**48.8±5.1 (10)**	**49.4±5.5 (11)**	53.3±6.7 (13)	44.6±9.5 (21)	46.9±7.7 (16)	44.3±2.4 (5)

Table 5.1: *Effect of changing myofiber orientation in the borderzone of the infarction on active myofiber stress. Presented are transmural average, $\overline{T}_a$, and standard deviation of the time averaged active stress during ejection for the five borderzone locations and the remote location. Reference (FibREF) and changed myofiber orientations (Fib*1.1, Fib*0.9, Fib+10, Fib-10) were incorporated in the model. The value between the brackets, IH indicates the transmural inhomogeneity of the stress distribution, quantified by the standard deviation of $\overline{T}_a$ expressed as a percentage of mean stress. Note that the change in myofiber orientation was only applied in the borderzone, i.e. at locations 1 to 5.*

5.4 Discussion

A numerical model of myofiber mechanics in the wall of the infarcted heart was developed. Active myofiber stress was evaluated in the region adjacent to a chronic infarction in response to variations in the local distribution of myofiber orientation.

In the model, the infarcted region was modelled as a stiff, non-contractile region. The experimentally observed stiffening of an infarct was simulated by a five times stiffening of the infarcted material (45; 58; 72). In the (stiffened) passive tissue, the direction of anisotropy and the anisotropy ratio were kept unchanged with respect to the pre-infarct situation. This choice was reasonable, since experiments by Zimmerman *et al.* indicate that large scar collagen fibers develop in the infarcted region, using the original structure as a scaffold (111).

In the present study element size was rather large as compared to the simulated infarct size. Only 63 (6%) of the 1071 nodes of the mesh were located within the infarcted region, and 126 (12%) of the nodes were located within the borderzone adjacent to the infarction where local myofiber orientation was varied. Since infarct size is small as compared to element size, within some elements both infarct and borderzone regions were present. Due to interpolation the transition between infarct and borderzone region was smooth. Similarly, the transition between borderzone and normal tissue was smooth as well. Increase of spatial resolution by mesh refinement was not convenient within the limits of acceptable calculation times. With the current mesh, calculations were performed in about 12 hours. With double resolution, each calculation would have taken about four days. Infarct size was kept small in agreement with the experiments (Chapter 4).

Myofibers running parallel to the infarcted region exhibit elevated active myofiber stress, a behavior opposite to myofibers running in series with this region. Due to the helical myofiber organization, endo- and epicardial myofibers are affected differently by the presence of an infarction. For locations 1 and 2, the epicardial myofibers are in series with the infarcted region. Consequently, mean active myofiber stress during ejection is low in this region. In the endocardial layers on the other hand, myofibers are running parallel to the infarcted region, causing elevation of active myofiber stress. At the other side of the infarction, at locations 4 and 5, effects are opposite. A similar effect was observed in a numerical study on borderzone mechanics around an acute myocardial infarction, which was modelled as a non-contractile region with no change in passive stiffness (13).

The homogeneity of the active myofiber stress distribution as found in the remote region (R) could be approached in the borderzone region by a change in offset, rather than a change in slope, of the transmural course of the helix angle. This offset change indicates a transmural rigid body rotation of myofibers in the borderzone. Local changes in the offset of the transmural course of the helix angle by about 10° however, appeared not to be sufficient to completely restore homogeneity of active myofiber stress. However, since our aim was to identify the trends in stress distribution changes due to local myofiber reorientation, it was not evaluated whether the inhomogeneity of 5% that was observed remote from the infarct region could be approached by a further change of offset or a combination of offset and slope changes. The direction of the adaptive myofiber reorientation necessary to restore homogeneity is dependent on position relative to the infarcted region.

Active myofiber stress appeared to be distributed rather homogeneously around the infarction. Except for location 3, all locations showed normal active myofiber stress values $\overline{T}_a$. At location 3, changing the offset of the transmural course of the helix angle by about 10° appeared to revert active myofiber stress to normal.

In experiments no significant changes in local myofiber orientation around a chronic infarction were found (Chapter 4). In these experiments however, mainly the well determined slope of the transmural course of the helix angle was studied. The transmural position where the helix angle changes sign was used as a reference. Therefore, offset changes could not be studied. Experimentally, an offset cannot be easily determined because of inaccuracies in estimating the long axis direction. The latter inaccuracies have a one to one effect on the offset of the helix angle. Near the apex, the local long axis direction is inherently ill-defined and sensitive to errors. Further away from the apex the long axis direction can be determined more accurately, with maximally expected alignment errors between the true LV long axis and our estimation of about ±10°. Furthermore, the accuracy of the used measurement technique itself was limited to about ±6°. Because of both effects, adaptive offset changes of the myofiber orientation on the order of ±10° can not be determined reliably.

5.5 Conclusion

In a simulation of the mechanics of a cardiac wall with a chronic transmural infarction the transmural distribution of active myofiber stress was three times more inhomogeneous in the borderzone adjacent to the infarction than in the remote region. In myofibers running parallel to the infarcted region active stress appears to be elevated, while in myofibers running in series with the infarction this stress is lowered.

Inhomogeneity of active myofiber stress in the borderzone could be compensated by transmural rigid body rotation on the order of 10° of the myofibers in the wall in patches near the infarct. Such small changes in myofiber orientation, and especially offset changes, however, are hard to detect by current methods for measurement of fiber direction.

We conclude that homogeneity of mechanical load in the borderzone of a transmural myocardial infarct can be restored by myofiber reorientation. This reorientation remains however below the level of detection for most measuring and analyzing methods of myofiber orientation.

Chapter 6

General discussion

6.1 Introductory remarks

The normal heart is able to adapt to changes in mechanical load, in order to generate the required pump function (40). The adaptive process tends to normalize mechanical load in the cardiac wall. It is clear that a change in wall mass or wall mass distribution is one of the adaptive changes that may occur. Other possible adaptive responses might involve changes in material properties (74; 85), or myofiber orientation (97; 109).

The aim of the present thesis was to investigate the hypothesis that myofiber reorientation in the cardiac wall provides an adaptive mechanism to maintain an optimal mechanical load for the myofibers in the cardiac wall. A combined approach was chosen, involving both animal experiments and finite element modelling of cardiac mechanics. In the experiments, local mechanical load was disturbed by induction of a transmural infarction. Ten weeks after infarct induction the resulting myofiber orientation in the normally perfused region adjacent to the infarction (borderzone) was measured. Comparisons were made with myofiber orientation in corresponding regions of normal hearts. The finite element model was used to estimate the mechanical load in the borderzone region. Besides, the amount of myofiber reorientation needed to restore homogeneity of mechanical load in the borderzone region was evaluated.

6.2 Measurement of myofiber orientation

Previous studies reported large variations in the distribution of normal myofiber orientation (39; 68; 82; 91; 93). Firstly, these variations may be attributed in part to the employed histological technique. The histological technique requires that myofibers should be traced over a certain distance within the tissue, implying that the tissue must be sliced such that the myofibers are parallel to the cutting plane. Inherently, this condition is cumbersome because the fiber direction in not known yet. In a well-cut slice the in-plane myofiber orientation can be measured accurately, but a possible out-of-plane component remains unknown. Secondly, the myofiber orientation as measured in a slice has to be referred to an anatomically determined coordinate system, which introduces reconstruction errors. In an attempt to minimize these errors, Nielsen *et al.* (68) measured the fiber direction on superficial layers of the left ventricle (LV), going from the epicardial wall to the endocardium by slicing the tissue parallel to the surface. The long axis of the left ventricle could thus be used as the common long axis. In this way, however, the myofibers were often not parallel to the measurement plane,

which probably limited the accuracy by which the in-plane angle could be measured. Moreover, the definition of the long axis direction is difficult since the real LV is not rotationally symmetric. Thirdly, myofiber orientations are usually reported as a function of transmural position, that is normalized with respect to local wall thickness. This procedure also contributes to the variation between different hearts, since detecting the endocardial wall is difficult due to its irregular shape.

In this study, Magnetic Resonance Diffusion Tensor Imaging (MR-DTI) was used to measure the distribution of myofiber orientation. Main advantage of this technique over histological methods is the possibility to measure true 3-dimensional myofiber orientation in the intact *post mortem* heart. Furthermore, to convert the measured absolute myofiber orientations to orientations relative to the cardiac wall, a novel definition of a local coordinate system was introduced. This coordinate system was based upon characteristics of the myofiber field and could be applied objectively, thus avoiding inter-observer variability. Finally, we used a new normalization technique. The transmural coordinate was normalized relative to the radius (R_0) at which the myofibers were in plane with the short-axis cross-section. The latter radius of normalization is better defined than the commonly used wall thickness, which is dependent on the detection of the endocardial wall. A first advantage of the use of R_0 is that the midwall surface determined by R_0 has a smooth appearance and is much better defined than the endocardial wall. More important however is the avoiding of errors in the offset of the transmural course of myofiber orientation, originating from errors in the estimate of the local long axis direction. However, by normalizing to the radius with zero out-of-plane myofiber component, changes in offset in the transmural course of the myofiber orientation, e.g. due to adaptation, cannot be detected anymore.

Using MR-DTI and the novel definition of the normalized wall-bound coordinate system, within a heart, myofiber orientation could be measured with an accuracy of 4.5°, which is better than obtained with histological methods (10°) (93; 82). Between different hearts, fiber orientation coincided within 6° (SD for n=5). This variation is low as compared to variation in earlier reports.

Both with histology and MR-DTI myofiber orientation can be measured reliably only in the *post mortem* state. Thus, a longitudinal study of myofiber reorientation is not possible. To evaluate whether myofiber orientation has changed, myofiber orientation in the infarcted hearts had to be compared to a reference of normal myofiber orientation obtained in normal hearts of an other group.

6.3 Animal model

To investigate myofiber reorientation, mechanical load had to be manipulated with no side effects and high rate of survival. We considered several options to manipulate local mechanical load, such as cardiac pacing, immobilization or dissection of part of the cardiac wall and induction of an infarction. Cardiac pacing was rejected as an intervention because it may lead to side effects to the changes in local mechanical load. Especially, in cardiac pacing the changes in timing between the electrical and mechanical events are not yet completely understood. Besides, to simulate this intervention in a numerical model, a model for the depolarization of the myocardium should be available. Immobilization or dissection of part of the cardiac wall is a difficult procedure with high risk of additional unknown damage. Therefore, we chose to vary local mechanical load by induction of an infarction. The infarctions had to be relatively small ($< 20\%$ of LV midwall affected surface) in order to avoid progression into cardiac failure.
After having selected the intervention, the choice for an animal model had to be made. The animal's heart had to be large enough to allow measurement of myofiber orientation with sufficient spatial accuracy. Moreover, a predictable and reproducible infarction had to be induced, which is facilitated when the number of coronary artery collaterals is scarce. Furthermore, an animal with a well developed Purkinje system was preferred, to diminish the risk of arrhythmia due to infarction. Finally, it was essential that there was experience with the selected animal in our lab. An animal which matched all these requirements was the goat (17; 62).
Finally, the timing of the intervention had to be determined. A period of 10 weeks was chosen to allow development of changes in cardiac tissue structures. Scar tissue formation in the infarcted region mainly takes place during the first 6 weeks (55). After this period a period of 4 weeks was added to allow adjustment of the tissue in the border zone to the mechanical tethering caused by the stiff infarction. It is unknown whether a steady state is present at the moment of sacrifice, since the time needed for the various adaptive processes in the heart remains largely unknown. Polarized light studies by Whittaker *et al.* (109) indicated that myofiber disarray occurred in the cardiac muscle tissue adjacent to the infarction as early as one week after infarct induction. Tezuka *et al.* reported a significant decrease in the fraction of circumferential fibers in the RV outflow tract in response to RV pressure overload within 28 to 81 days (97).

6.4 Numerical model of cardiac mechanics

A numerical model of cardiac mechanics was used to investigate the characteristics of local myofiber reorientation needed to restore homogeneity of mechanical load in the borderzone adjacent to a chronic infarction.
In the model, the infarcted region was modelled as stiff and non-contractile. Information on stiffening of the infarct region is limited. In the present simulations, the infarct was five times as stiff relative to the normal passive elastic tissue, thus preventing severe stretch of the infarct tissue. Infarct material properties seem however not to be critical. In a previous study (13), an acutely ischemic region was simulated as a non-contractile region, having normal passive material stiffness. In the latter simulation it was also found that active stress was higher in myofibers running parallel to the infarcted region and lower in myofibers running in series with this region. It is therefore expected that myofiber reorientation as found in our study is moderately dependent on material properties of the infarct, as long as passive stiffness in the infarct region is much lower than active stiffness generated by the viable myofibers.
Which mechanical parameter serves as stimulus for adaptation is still a matter of debate. In this study homogeneity of active stress during ejection was used as a criterion to evaluate the effect of myofiber reorientation. This parameter was used because 1) fiber stress is closely related to local cardiac function, and 2) mean fiber stress appeared not sensitive to the used activation sequence (12). A recent study, using a numerical model of cardiac mechanics and oxygen consumption, indicates that the optimal myofiber orientations found for either homogeneous active myofiber stress, homogeneous myofiber strain, or homogeneous ATP consumption closely coincide (104). These results indicate that myofiber strain, active myofiber stress as well as ATP consumption could serve as a stimulus for adaptation.

6.5 Cardiac myofiber reorientation: A mechanism for adaptation?

To provide an adaptive mechanism, myofiber reorientation must contribute to the restoration of homogeneity of mechanical load in the borderzone. In our animal model of cardiac infarction, no significant differences in myofiber orientation in the borderzone region were detected. The latter finding may be explained as follows: 1) myofibers do not have the ability to reorient, or

2) homogeneity of mechanical load in the border zone cannot be restored by myofiber reorientation, or 3) myofiber reorientation did occur, but the amount of reorientation remained below the level of detection with the MR-DTI technique.

The first possibility, that myofibers cannot reorient, is contradicted by experiments. Myofiber reorientation appears to be possible by two different mechanisms. Active myofiber reorientation, where muscle cells actively rearrange their connections to other cells, has been reported to occur at the borderzone of the rat myocardial infarction (63). Also around infarcted regions, myofiber disarray was observed (66; 109). Although myofiber disarray can hardly be regarded as a successful adaptive process, it illustrates the possibility of myofiber reorientation. Furthermore, myofiber reorientation may also be the result of a passive adaptive process, where reorientation of cardiac myofibers is to be attributed to changes in the passive matrix. It has been shown that elevated stress and strain may lead to rupture of the passive matrix (34). In the borderzone of an acute infarction elevated shear strain has been measured (65). When locally the passive matrix is ruptured by these high shear strains, rotation of the myofibers may occur.

In a numerical model of cardiac mechanics, it was investigated whether restoration of homogeneity of mechanical load through myofiber reorientation was basically impossible, or whether myofiber reorientation would remain below the level of detection. In the model it appeared that, due to the presence of the infarction, inhomogeneity of transmural active myofiber stress in the borderzone adjacent to the infarction increased from 5 to 15%. This inhomogeneity could be compensated by a rigid body rotation on the order of 10° of the myofibers in transmural patches near the infarct.

Therefore, myofiber reorientation is not ruled out as an adaptive mechanism by which homogeneity of mechanical load is restored in the borderzone of a myocardial infarct. However, for an infarcted region of about 10% of total LV wall mass, the magnitude and characteristics of reorientation needed to restore homogeneity of workload, are near the detection limit of current methods for measuring and analysis of myofiber orientation.

6.6 Conclusion

In this thesis the hypothesis was investigated that myofiber reorientation in the cardiac wall provides an adaptive mechanism to maintain an optimal mechanical load for the myofibers in the cardiac wall.
In experiments on goat hearts, myofiber orientation was measured in three dimensions, using Magnetic Resonance Diffusion Tensor Imaging (MR-DTI). Within a heart, myofiber orientation was measured with an accuracy of 4.5°. Between five hearts, myofiber orientation varied around a common pattern by about ±6°, a variation which is much less than reported in many previous studies. In the left ventricle the common pattern is in agreement with earlier findings. Furthermore, at midwall a transverse component of myofiber orientation, quantifying the cross-over of myofibers through the wall, was found varying monotonously from apex to base, changing sign near the equator. The found common myofiber structure agreed quite well with model predictions, based upon the assumption that myofiber direction adapts until stress and strain during the ejection phase are homogeneous within the cardiac wall.
Next, it was investigated whether reported variations in myofiber orientation could be explained by biological variation in geometry. It was expected that the distribution of myofiber orientations for which stresses during ejection are homogeneous throughout the cardiac wall depends on geometric properties. In simulations it was found that occurring biological variations in geometry needed compensations of fiber orientation by generally less than 10°. The large variations as reported in literature cannot be attributed to this adaptation. More likely, the reported variations are related to poor definition of a coordinate system, which was based generally on the external geometry of the left ventricle. In the present study, variation in myofiber orientation was probably so small, because the used coordinate system was well-defined. It was largely based on the geometry of a midwall surface, where myofibers were in plane with the short-axis cross-section.
The general hypothesis of this thesis was investigated in an animal model of chronic infarction. In goat hearts with an infarcted region of about 10% of LV wall mass, myofiber orientation in the borderzone was measured 10 weeks after infarct induction. Despite changes in mechanics in the border zone adjacent to the infarction, myofiber orientation was not measured to vary significantly in this region. In simulations of cardiac adaptation to changes in mechanical load after an infarction, myofibers in the borderzone were expected to change orientation by about 10°. These simulation results thus confirm that changing

myofiber orientation is a potentially effective tool to redistribute mechanical load in the cardiac wall. It may be so effective that the needed reorientation is too small to be detected reliably with current methods of measurement and of analysis. We therefore conclude that the hypothesis that myofiber reorientation in the cardiac wall provides an adaptive mechanism to maintain an optimal mechanical load may not be rejected.

References

[1] A.M. Abdulla, M.J. Frank, M.I. Canedo, and M.A. Stefadouros. Limitations of echocardiography in the assessment of left ventricular size and function in aortic regurgitation. *Circulation*, 61(1):148–155, 1980.

[2] G.E. Adomian and J.W. Beazell. Myofibrillar disarray produced in normal hearts by chronic electrical pacing. *Am Heart J.*, 112(1):79–83, 1986.

[3] T. Arts, P.H.M. Bovendeerd, F.W. Prinzen, and R.S. Reneman. Relation between left ventricular cavity presure and volume and systolic fiber stress and strain in the wall. *Biophys J.*, 59:93–103, 1991.

[4] T. Arts, F.W. Prinzen, L.H.E.H. Snoeckx, J.M. Rijcken, and R.S. Reneman. Adaptation of cadiac structure by mechanical feedback in the environment of the cell: A model study. *Biophys J.*, 66:953–961, april 1994.

[5] T. Arts, P.C. Veenstra, and R.S. Reneman. A model of the mechanics of the left ventricle. *Ann Biomed Eng.*, 7:299–318, 1979.

[6] T. Arts, P.C. Veenstra, and R.S. Reneman. Epicardial deformation and left ventricular wall mechanics during ejection in the dog. *Am J Physiol.*, 243:H379–H390, 1982.

[7] P.J. Basser, J. Matiello, and D. LeBihan. MR diffusion tensor spectroscopy and imaging. *Biophys J.*, 66:259–267, 1994.

[8] P.J. Basser and C. Pierpaoli. Microstructural and physiological features of tissues elucidated by quantitative-diffusion-tensor mri. *J Magn Reson., Ser B*, 111:209–219, 1996.

[9] R. Beyar and S. Sideman. A computer study of the left ventricular performance based on fiber structure, sarcomere dynamics, and transmural electrical propagation velocity. *Circ Res.*, 55:358–375, 1984.

[10] B. Bhusnurmath, B.N. Datta, H.N. Khattri, R.P. Sapru, and P.L. Wahi.

Myocardial infarction at autopsy: Morphologic observations on 272 cases. *Indian Heart J*, 37(6):353–360, 1985.

[11] E.A. Bocchi, L.F. Moreira, A.V. de Moraes, G. Bellotti, M. Gama, N.A.G. Stolf, A.D. Jatene, and F. Pileggi. Effects of dynamic cadiomyoplasty on regional wall motion, ejection fraction and geometry of the left ventricle. *Circulation*, 86, supp II:II231–II235, 1992.

[12] P.H.M. Bovendeerd. *The mechanics of the normal and ischemic left ventricle during the cardiac cycle - a numerical and experimental analysis.* PhD thesis, Maastricht University, Maastricht, The Netherlands, october 1990.

[13] P.H.M. Bovendeerd, T. Arts, T. Delhaas, J.M. Huyghe, D.H. van Campen, and R.S. Reneman. Regional wall mechanics in the ischemic left ventricle: numerical modeling and dog experiments. *Am J Physiol.*, 270:H398–H410, 1996.

[14] P.H.M. Bovendeerd, T. Arts, J.M. Huyghe, D.H. van Campen, and R.S. Reneman. Dependence of local left ventricular wall mechanics on myocardial fiber orientation: A model study. *J Biomech.*, 25(10):1129–1140, 1992.

[15] P.H.M. Bovendeerd, J.M. Huyghe, T. Arts, D.H. van Campen, and R.S. Reneman. Influence of endocardial-epicardial crossover of muscle fibers on left ventricular wall mechanics. *J Biomech.*, 27(7):941–951, 1994.

[16] P.H.M. Bovendeerd, J. Rijcken, D.H. van Campen, A.J.G. Schoofs, K. Nicolay, and T. Arts. Optimization of left ventricular muscle fiber orientation. *Proc IUTAM, Denmark*, pages 285–295, 1998.

[17] W.E. Brown, M.G. Magno, P.D. Buckman, F. Di Meo, D.R. Gale, and J.D. Mannion. The coronary collateral circulation in normal goats. *J Surg Res.*, 51:54–59, 1991.

[18] B.A. Carabello, M.R. Zile, R. Tanaka, and G. Cooper IV. Left ventricular hypertrophy due to volume overload versus pressure overload. *Am J Physiol.*, 263:H1137–H1144, 1992.

[19] T.E. Carew and J.W. Covell. Fiber orientation in hypertrophied canine left ventricle. *Am J Physiol.*, 236(3):H487–H493, 1979.

[20] J.B. Caulfield and T.K. Borg. The collagen network of the heart. *Lab Invest.*, 40(3):364–372, 1979.

[21] J.B. Caulfield and J.S. Janicki. Structure and function of myocardial fibrillar collagen. *Technol Healt Care*, 5:95–113, 1997.

[22] R.S. Chadwick. Mechanics of the left ventricle. *Biophys J.*, 39:279–288, 1982.

[23] K.D. Costa, P.J. Hunter, J.M. Rogers, J.M. Guccione, L.K. Waldman, and A.D. McCulloch. A three-dimensional finite element method for large elastic deformations of ventricular myocardium: I—cylindrical and spherical polar coordinates. *J Biomech Eng.*, 118:452–463, november 1996.

[24] K.D. Costa, P.J. Hunter, J.S. Wayne, L.K. Waldman, J.M. Guccione, and A.D. McCulloch. A three-dimensional finite element method for large elastic deformations of ventricular myocardium: Ii—prolate spheroidal coordinates. *J Biomech Eng.*, 118:464–473, november 1996.

[25] S.C. Cowin. Strain or deformation rate dependent finite growth in soft tissues. *J Biomech.*, 30(5):647–649, 1996.

[26] M.M. Cox, I. Berman, R.J. Myerbrug, M.J.D. Smets, and P.L. Kozlovskis. Morphometric mapping of regional myocyte diameters after healing of myocardial infarction in cats. *J Mol Cell Cardiol.*, 23:127–135, 1991.

[27] L.M.D. Delbridge, H. Satoh, W. Yuan, J.W.M. Bassani andM. Qi, K.S. Ginsburg, A.M. Samarel, and D.M. Bers. Cardiac myocyte volume, ca^{2+} fluxes, and sarcoplasmic reticulum loading in pressure-overload hypertrophy. *Am J Physiol.*, 272:H2425–H2435, 1997.

[28] S.-J. Dong, P.S. Hees, W.-M. Huang, S.A. Buffer, J.L. Weiss, and E.P. Shapiro. Independent effects of preload, afterload, and contractility on left ventricular torsion. *Am J Physiol.*, 277:H1053–H1060, 1999.

[29] G.M. Drzewiecki, E. Karam, J.K-J. Li, and A. Noordergraaf. Cardiac adaptation of sarcomere dynamics to arterial load: a model of hypertrophy. *Am J Physiol.*, 263:H1054–1063, 1992.

[30] J. Dusek. Significance of morphological changes at the periphery of an experimental myocardial infarct. *Recent Adv Stud Cardiac Struct Metab.*, 1:430–438, 1972.

[31] J. Dusek, G. Rona, and D.S. Kahn. Healing process in the marginal zone of an experimental myocardial infarct. *Am J Pathol.*, 62(3):321–338, 1971.

[32] W.D. Edwards. Applied anatomy of the heart. In E.R. Giuliani, V. Fuster, B.J. Gersh, M.D. McGoon, and D.C. McGoon, editors, *Cardiology — Fundamentals and practice.* 2nd *edition*, chapter 4, pages 47–112. Mosby Year Book, 1991.

[33] J.L. Emery and J.H. Omens. Mechanical regulation of myocardial growth during volume-overload hypertrophy in the rat. *Am J Physiol.*, 273:H1198–H1204, 1997.

[34] J.L. Emery, J.H. Omens, and A.D. McCulloch. Strain softening in rat left ventricular myocardium. *J Biomech Eng.*, 119:6–12, february 1997.

[35] R.H. Fagard. Impact of different sports and training on cardiac structure and function. *Cardiol Clin.*, 15(3):397–412, 1997.

[36] L. Garrido, V.J. Wedeen, K.K. Kwong, U.M. Spencer, and H.L. Kantor. Anisotropy of water diffusion in the myocardium of the rat. *Circ Res.*, 74:789–793, 1994.

[37] J.J. Gomez-Doblas, J. Schor, P. Vignola, D. Weinberg, E. Traad, R. Carrillo, D. Williams, and G.A. Lamas. Left ventricular geometry and operative mortality in patients undergoing mitral valve replacement. *Clin Cardiol*, 24:717–722, 2001.

[38] G.J. Gottlieb, S.H. Kubo, and D.R. Alonso. Ultrastructural characterization of the border zone surrounding early experimental myocardial infarcts in dogs. *Am J Pathol.*, 103:292–303, 1981.

[39] R.A. Greenbaum, S.Yen Ho, D.G. Gibson, A.E. Becker, and R.H. Anderson. Left ventricular fibre architecture in man. *Br Heart J.*, 45:248–263, 1981.

[40] W. Grossman. Cardiac hypertrophy: Useful adaptation or pathologic process? *Am J Med*, 69:576–584, 1980.

[41] W. Grossman, D. Jones, and L.P. McLaurin. Wall stress and patterns of hypertrophy in the human left ventricle. *J Clin Invest.*, 56:56–64, 1975.

[42] J.M. Guccione, K.D. Costa, and A.D. McCulloch. Finite element stress analysis of left ventricular mechanics in the beating dog heart. *J Biomech.*, 28(10):1167–1177, 1995.

[43] K.B. Gupta, M.B. Ratcliffe, M.A. Fallert, L.H. Edmunds, and D.K. Bogen. Changes in passive mechnical stiffness of myocardial tissue with aneurysm formation. *Circulation*, 89:2315–2326, 1994.

[44] G. Hasenfuss. Animal models of human cardiovascular disease, heart failure and hypertrophy. *Cardiovasc Res.*, 39:60–76, 1998.

[45] J.W. Holmes, J.A. Nunez, and J.W. Covell. Functional implications of myocardial scar structure. *Am J Physiol.*, 272:H2123–H2130, 1997.

[46] J.W. Holmes, D.F. Scollan, and R.L. Winslow. Direct histological validation of diffusion tensor mri in formaldehyde-fixed myocardium. *Magn Reson Med.*, 44:157–161, 2000.

[47] E.W. Hsu, A.L. Muzikant, S.A. Matulevicius, R.C. Penland, and C.S. Henriques. Magnetic resonance myocardial fiber-orientation mapping with direct histological correlation. *Am J Physiol.*, 274:H1627–H1634, 1998.

[48] J.C.M. Hsu, F.A. Johnson, W.M. Smith, K.A. Reimer, and R.E. Ideker. Magnetic resonance imaging of chronic myocardial infarcts in formalin-fixed human autopsy hearts. *Circulation*, 89:2133–2140, 1994.

[49] R.M. Huisman, G. Elzinga, and N. Westerhof. Measurement of left ventricular wall stress. *Cardiovasc Res.*, 14:142–153, 1980.

[50] P.J. Hunter, A.D. McCulloch, and H.E.D.J. ter Keurs. Modelling the mechanical properties of cardiac muscle. *Prog Biophys Mol Bio.*, 69:289–331, 1998.

[51] P.J. Hunter, M.P. Nash, and G.B. Sands. Computational electromechanics of the heart. In A.V. Panfilov and A.V. Holden, editors, *Computational biology of the heart.*, chapter 12, pages 345–407. John Wiley and Sons, Ltd., 1997.

[52] P.J. Hunter, B.H. Smaill, P.M.F. Nielsen, and I.J. LeGrice. A mathematical model of cardiac anatomy. In A.V. Panfilov and A.V. Holden, editors, *Computational biology of the heart.*, chapter 6, pages 171–216. John Wiley and Sons, Ltd., 1997.

[53] R. Jacob and R.W. Guelch. The functional significance of ventricular geometry for the transition from hypertrophy to cardiac failure. does a critical degree of structural dilatation exist? *Basic Res Cardiol.*, 93:423–429, 1998.

[54] D.K. Jones, M.A. Horsfield, and A. Simmons. Optimal strategies for measuring diffusion in anisotropic systems by magnetic resonance imaging. *Magn Reson Med.*, 42:515–525, 1999.

[55] B.I. Jugdutt and M.I. Khan. Impact of increased infarct transmurality on remodeling and function during healing after anterior myocardial infarction in the dog. *Can J Physiol Pharm.*, 70:949–958, 1992.

[56] P.P. Karpawich, C.D. Justice, D.L. Cavitt, and C.-H. Chang. Developmental sequelae of fixed-rate ventricular pacing in the immature canine heart: An electrophysiologic, hemodynamic, and histopathologic evaluation. *Am Heart J.*, 119:1077–1083, 1990.

[57] P.P. Karpawich, C.D. Justice, C.-H. Chang, C.Y. Gause, and L.R. Kuhns. Septal ventricular pacing in the immature canine heart: A new perspective. *Am Heart J.*, 121:827–833, 1991.

[58] C.M. Kramer, J.A.C. Lima, N. Reichek, V.A. Ferrari, M.R. Llaneras, L.C. Palmon, I-T Yeh, B. Tallant, and L. Axel. Regional differences in function within noninfarcted myocardium during left ventricular remodeling. *Circulation*, 88:1279–1288, 1993.

[59] C.M. Kramer, W.J. Rogers, C.S. Park, S. Seibel, A. Shaffer, T.M. Theobald, N. Reichek, T. Onodera, and A.M. Gerdes. Regional myocyte hypertrophy parallels regional myocardial dysfunction during post-infarct remodeling. *J Mol Cell Cardiol.*, 30:1773–1778, 1998.

[60] D. LeBihan. Molecular diffusion NMR imaging. *Magn Reson Q.*, 7:1–30, 1991.

[61] I-E. Lin and L.A. Taber. A model for stress-induced growth in the developing heart. *J Biomech Eng.*, 117:343–349, august 1995.

[62] G. Lipovetsky, J.J. Fenoglio, M. Gieger, M.R. Srinivasan, and W.H. Dobelle. Coronary artery anatomy of the goat. *Artif Organs.*, 7(2):238–245, 1983.

[63] T. Matsushita, M. Oyamada, K. Fujimoto, Y. Yasuda, S. Masuda, Y. Wada, T. Oka, and T. Takamatsu. Remodeling of cell-cell and cell-extracellular matrix interactions at the borderzone of rat myocardial infarcts. *Circ Res.*, 85:1046–1055, 1999.

[64] R. Mazhari, J.H. Omens, J.W. Covell, and A.D. McCulloch. Structural basis of regional dysfunction in acutely ischemic myocardium. *Cardiovasc Res.*, 47:284–293, 2000.

[65] R. Mazhari, J.H. Omens, L.K. Waldman, and A.D. McCulloch. Regional myocardial perfusion and mechanics: A model-based method of analysis. *Ann Biomed Eng.*, 26:743–755, 1998.

[66] J. Milei, R. Migliore, F. Guerrero, C. Pedroza, and R. Storino. Muslce fiber disarray in patients without hypertrophic cardiomyopathy. *Cardiology*, 72:105–112, 1985.

[67] M. Nahrendorf, F. Wiesmann, K-H. Hiller, K. Hu, C. Waller, J. Ruff, T.E. Lanz, S. Neubauer, A. Haase, G. Ertl, and W.R. Bauer. Serial cine-magnetic resonance imaging of left ventricular remodeling after myocardial infarction in rats. *JMRI*, 14:547–555, 2001.

[68] P.M.F. Nielsen, I.J. LeGrice, B.H. Smaill, and P.J. Hunter. Mathematical model of geometry and fibrous structure of the heart. *Am J Physiol.*, 260:H1365–H1378, 1991.

[69] G. Olivetti, R. Ricci, C. Lagrasta, E. Maniga, E.H. Sonnenblick, and P. Anversa. Cellular basis of wall remodeling in long-term pressure

overload-induced right ventricular hypertrophy in rats. *Circ Res.*, 63:648–657, 1988.

[70] J.H. Omens. Stress and strain as regulators of myocardial growth. *Prog Biophys Mol Bio.*, 69:559–572, 1998.

[71] J.H. Omens and J.W. Covell. Transmural distribution of myocardial tissue growth induced by volume-overload hypertrophy in the dog. *Circulation*, 84:1235–1245, 1991.

[72] W.W. Parmley, L. Chuck, C. Kivowitz, J.M. Matloff, and H.J.C. Swan. In vitro length-tension realtions of human ventricular aneurysms — relation of stiffness to mechanical disadvantage. *Am J Cardiol*, 32(7):889–894, 1973.

[73] V.S. Paukov, V.A. Frolov, and T.M. Yudakova. Changes in the ultrasturcture of the "intact" zone of heart muscle and contractile activity of the heart in acute myocardial ischemia. *B Exp Biol Med+*, 77(6):604–607, 1974.

[74] E.S. Pearlman, K.T. Weber, J.S. Janicki, G.G. Pietra, and A.P. Fishman. Muscle fiber orientation and connective tissue content in the hypertrophied human heart. *Lab Invest.*, 46(2):158–164, 1982.

[75] C.S. Peskin. Fiber architecture of the left ventricular wall: An asymptotic analysis. *Commun Pure Appl Math.*, 42:79–113, 1989.

[76] F.W. Prinzen, T. Arts, A.P.G. Hoeks, and R.S. Reneman. Discrepancies between myocardial blood flow and fiber shortening in the ischemic border zone as assessed with video mapping of epicardial deformation. *Pflugers Arch.*, 415:220–229, 1989.

[77] F.W. Prinzen, E.C. Cheriex, T. Delhaas, M.F.M. van Oosterhout, T. Arts, H.J.J. Wellens, and R.S. Reneman. Asymmetric thickness of the left ventricular wall resulting from asynchronous electric activation: A study in dogs with ventricular pacing and in patients with left bundle branch block. *Am Heart J.*, 130:1045–1053, 1995.

[78] T.G. Reese, R.M. Weisskoff, R.N. Smith, B.R. Rosen, R.E. Dinsmore, and V.J. Wedeen. Imaging myocardial fiber architecture in vivo with magnetic resonance. *Magn Reson Med.*, 34:786–791, 1995.

[79] J. Rijcken, P.H.M. Bovendeerd, A.J.G. Schoofs, D.H. van Campen, and T. Arts. Optimization of cardiac fiber orientation for homogeneous fiber strain at beginning of ejection. *J Biomech.*, 30:1041–1049, 1997.

[80] J. Rijcken, P.H.M. Bovendeerd, A.J.G. Schoofs, D.H. van Campen, and T. Arts. Optimization of cardiac fiber orientation for homogeneous fiber strain during ejection. *Ann Biomed Eng.*, 27:289–297, 1999.

[81] E.K. Rodriguez, A. Hoger, and A.D. McCulloch. Stress-dependent finite growth in soft elastic tissues. *J Biomech.*, 27(4):455–467, 1994.

[82] M.A. Ross and D.D. Streeter. Nonuniform subendocardial fiber orientation in the normal macaque left ventricle. *Eur J Cardiol.*, 3(3):229–247, 1975.

[83] S.A. Rubin, M.C. Fishbein, H.J.C. Swan, and A. Rabines. Compensatory hypertrophy in the heart after myocardial infarction in the rat. *J Am Coll Cardiol.*, 1(6):1435–1441, 1983.

[84] J. Sadoshima and S Izumo. The cellular and molecular response of cardiac myocytes to mechanical stress. *Annu Rev Physiol.*, pages 551–571, 1997.

[85] S.M. Schwartz, D. Gordon, R.S. Mosca, E.L. Bove, K.P. Heidelberger, and T.J. Kulik. Collagen content in normal, pressure, and pressure-volume overloaded developing human hearts. *Am J Cardiol*, 77:734–738, 1996.

[86] D.F. Scollan, A. Holmes, R. Winslow, and J. Forder. Histological validation of myocardial microstructure obtained from diffusion tensor magnetic resonance imaging. *Am J Physiol.*, 275:H2308–H2318, 1998.

[87] D.F. Scollan, A. Holmes, J. Zhang, and R. Winslow. Reconstruction of cardiac ventricular geometry and fiber orientation using magnetic resonance imaging. *Ann Biomed Eng.*, 28:934–944, 2000.

[88] J.F. Spear, E.L. Michelson, and E.N. Moore. Cellular electrophysiologic characteristics of chronically infarcted myocardium in dogs susceptible to sustained ventricular tachyarrhythmias. *J Am Coll Cardiol.*, 1(4):1099–1110, 1983.

[89] E.O. Stejskal and J.E. Tanner. Spin diffusion measurements: spin echoes in the presence of a time-dependent field gradient. *J Chem Phys.*, 42:288–292, 1965.

[90] D.D. Streeter. Gross morphology and fiber geometry of the heart. In R.M.Berne, editor, *Handbook of physiology — The Cardiovascular system I.* American physiological society, 1979.

[91] D.D. Streeter and W.T. Hanna. Engineering mechanics for successive states in canine left ventricular myocardium — II. fiber angle and sarcomere length. *Circ Res.*, 33:656–664, 1973.

[92] D.D. Streeter, W.E. Powers, M.A. Ross, and F. Torrent-Guasp. Three-dimensional fiber orientation in the mammalian left ventricular wall. In

J. Baan, A. Noordergraaf, and J. Raines, editors, *Cardiovascular system dynamics.*, pages 73–84. Cambridge, Mass.: MIT Press, 1978.

[93] D.D. Streeter, H.M. Spotnitz, D.P. Patel, J. Ross, and E.H. Sonnenblick. Fiber orientation in the canine left ventricle during diastole and systole. *Circ Res.*, 24:339–347, 1969.

[94] Y. Sun and K.T. Weber. Infarct scar: a dynamic tissue. *Cardiovasc Res.*, 46:250–256, 2000.

[95] L.A. Taber. Biomechanics of growth, remodeling, and morphogenesis. *Appl Mech Rev*, 48(8):487–545, 1995.

[96] F. Tezuka. Muscle fiber orientation in normal and hypertrophied hearts. *Tohoku J Exp Med*, 117:289–297, 1975.

[97] F. Tezuka, W. Hort, P.E. Lange, and J.H. Nürnberg. Muscle fiber orientation in the development and regression of right ventricular hypertrophy in pigs. *Acta Pathol Jpn*, 40:402–407, 1990.

[98] F. Torrent-Guasp. *The cardiac muscle.* Fundacin Juan, Madrid, 1973.

[99] W.-Y.I. Tseng, T.G. Reese, R.M. Weisskoff, T.J. Brady, and V.J. Wedeen. Myocardial fiber shortening in humans: Initial results of mr imaging. *Radiology*, 216:128–139, 2000.

[100] W.-Y.I. Tseng, T.G. Reese, R.M. Weisskoff, and V.J. Wedeen. Cardiac diffusion tensor MRI in vivo without strain correction. *Magn Reson Med.*, 42:393–403, 1999.

[101] G.J. van der Vusse, T. Arts, J.F.C. Glatz, and R.S. Reneman. Transmural differences in energy metabolism of the left ventricular myocardium: Fact or fiction? *J Mol Cell Cardiol.*, 22:23–37, 1990.

[102] M.F.M van Oosterhout, F.W. Prinzen, T. Arts, J.J. Schreuder, W.Y.R. Vanagt, J.P.M Cleutjens, and R.S. Reneman. Asynchronous electrical activation induces asymmetrical hypertrophy of the left ventricular wall. *Circulation*, 98:588–595, 1998.

[103] M.F.M van Oosterhout H.M.M. Willigers, R.S. Reneman, and F.W. Prinzen. Fluorescent microspheres to measure organ perfusion: Validation of a simplified sample processing technique. *Am J Physiol.*, 269:H725–H733, 1995.

[104] M. Vendelin. *Cardiac mechanoenergetics in silico.* PhD thesis, Tallinn Technical University, Tallinn, Estonia, 2001.

[105] M. Vendelin, P.H.M. Bovendeerd, T. Arts, J. Engelbrecht, and D.H. van Campen. Cardiac mechanoenergetics replicated by cross-bridge model. *Ann Biomed Eng.*, 28:629–640, 2000.

[106] F.J. Vetter and A.D. McCulloch. Three-dimensional analysis of regional cardiac function: A model of rabbit ventricular anatomy. *Prog Biophys Mol Bio.*, 69:157–183, 1998.

[107] P.S. Vokonas, R. Gorlin, P.F. Crhon, M.V. Herman, and E.H. Sonnenblick. Dynamic geometry of the left ventricle in mitral regurgitation. *Circulation*, 48:786–795, 1973.

[108] N. Westerhof, G. Elzinga, and G.C. van den Bos. Influence of central and peripherical changes on the hydraulic input impedance of the systemic arterial tree. *Med Biol Eng.*, 11:710–723, 1973.

[109] P. Whittaker, D.R. Boughner, and R.A. Kloner. Analysis of healing after myocardial infarction using polarized light microscopy. *Am J Pathol.*, 134(4):879–893, 1989.

[110] S.A. Wickline, E.D. Verdonk, A.K. Wong, T.K. Shepard, and J.G. Miller. Structural remodeling of human myocardial tissue after infarction. *Circulation*, 85:259–268, 1992.

[111] S.D. Zimmerman, W.J. Karlon, J.W. Holmes, J.H. Omens, and J.W. Covell. Structural and mechanical factors influencing infarct scar collagen organization. *Am J Physiol.*, 278:H194–H200, 2000.

Appendix A

Appendix

A.1 Definition of reference myofiber orientation

To describe the spatial variation of the helix and transverse fiber angle, local normalized coordinates $\overline{\xi}$ and $\overline{\theta}$ are defined in a plane of constant circumferential position ϕ (figure 3.1). The normalized coordinate $\overline{\xi}$ varies linearly with the actual distance in the ventricular wall, from $\overline{\xi} = -1$ at the endocardial surface to $\overline{\xi} = +1$ at the epicardial surface. The normalized longitudinal coordinate $\overline{\theta}$ varies linearly with the distance from the equatorial plane, as measured along the meriodanal curve through the point of interest. It varies from +0.5 in the basal plane, through 0 at the equator to -1 at the apex. The polynomials that describe the helix angle, α_h, and the transverse angle, α_t are:

$$\begin{aligned}\alpha_h(\overline{\xi},\overline{\theta}) &= (h_{10}L_0(\overline{\xi}) + h_{11}L_1(\overline{\xi}) + h_{12}L_2(\overline{\xi}) + h_{13}L_3(\overline{\xi}) + h_{14}L_4(\overline{\xi})) \\ &\quad (1 + h_{22}L_2(\overline{\theta}) + h_{24}L_4(\overline{\theta})) \end{aligned} \tag{A.1}$$

$$\begin{aligned}\alpha_t(\overline{\xi},\overline{\theta}) &= (1 + t_{11}L_1(\overline{\xi}) + t_{12}L_2(\overline{\xi}))(1 - \overline{\xi}^2) \\ &\quad (t_{21}L_1(\overline{\theta}) + t_{23}L_3(\overline{\theta}) + t_{25}L_5(\overline{\theta})) \end{aligned} \tag{A.2}$$

where the polynomials $L_i(\overline{\xi})$ and $L_i(\overline{\theta})$ are Legendre polynomials of order i and the parameters h_{ij} and t_{ij} are the polynomial coefficients. Values of the fiber angle parameters for the reference fiber orientation (FibREF) are listed in table A.1.

h_{10}	h_{11}	h_{12}	h_{13}	h_{14}	h_{22}	h_{24}
rad	rad	rad	rad	rad	-	-
0.362	-1.16	-0.124	0.129	-0.0614	0.0984	-0.0701
t_{11}	t_{12}	t_{21}	t_{23}	t_{25}		
-	-	rad	rad	rad		
-0.626	0.502	0.501	0.169	0.0304		

Table A.1: *Fiber parameter values, as used in Rijcken (1999).*

A.2 Active constitutive behavior

Active behavior is described by a contractile element in series with a series elastic element (6; 14). The total length these two elements equals the sarcomere length l_s. The length of the contractile element equals l_c. The

model is formulated in terms of the first Piola-Kirchhoff stress T_a. The stress generated by the contractile element is transmitted by the series elastic element and given by:

$$T_a = E_a \, T_{max} \, (l_s - l_c) \tag{A.3}$$

The stiffness of the series elastic element is equal to $E_a T_{max}$, where E_a is a constant. T_{max} depends on l_c, l_s and the time t_s that has elapsed since the moment of onset of activation:

$$T_{max} = T_1 A_l(l_c) \, A_t(t_s, l_s) \tag{A.4}$$

A detailed description of equation A.4 can be found in (14). The contraction model is completed by an evolution equation for the contractile element length l_c, which reads:

$$\frac{\partial l_c}{\partial t} = (E_a(l_s - l_c) - 1)v_0 \tag{A.5}$$

Parameter settings for the model were adopted from (14).

Samenvatting

De pompfunctie van het hart wordt gegenereerd door contractie van de spiervezels in de hartwand. De bijdrage die iedere spiervezel levert aan de contractie, is sterk afhankelijk van de oriëntatie van de spiervezel in de hartwand. In een normaal hart varieert de spiervezeloriëntatie van de binnen- naar de buitenwand van het hart over ongeveer 120°.
De hartspier is in staat zich aan te passen aan veranderingen in de belasting om zo de bloedtoevoer naar de weefsels in stand te houden. Het proces van aanpassing aan de belasting wordt ook wel adaptatie genoemd. Het adaptieve proces zorgt ervoor dat de belasting in de hartwand voor alle spiervezels optimaal blijft, wat onder andere inhoudt dat de belasting gelijk verdeeld moet zijn over alle spiervezels. Eén manier waarop weefsels reageren op een verandering van de belasting is door te groeien. Het is echter waarschijnlijk dat er nog andere adaptieve mechanismen bestaan, zoals het aanpassen van de materiaaleigenschappen, of de spiervezeloriëntatie.
In dit proefschrift is de hypothese getoetst dat verandering van de spiervezeloriëntatie in het hart een adaptief mechanisme is waarmee de belasting van de spiervezels optimaal wordt gehouden.
Om deze hypothese te toetsen zijn zowel dierexperimenten als een numeriek model van de hartspiermechanica gebruikt. In de dierexperimenten hebben we de lokale mechanica verstoord door inductie van een hartinfarct bij geiten. Tien weken na aanbrengen van het infarct werd vervolgens de spiervezeloriëntatie gemeten in de zone die grensde aan het infarct (randzone). Deze spiervezeloriëntatie werd vervolgens vergeleken met de spiervezeloriëntatie zoals die in overeenkomstige zones in gezonde harten werd gemeten. Met behulp van het numerieke model kon een schatting worden gemaakt van de mechanische belasting in de randzone. Bovendien werd onderzocht welke verandering van de spiervezeloriëntatie nodig was om de belasting in de randzone van het infarct weer gelijkmatig verdeeld te krijgen. Spiervezeloriëntatie kan alleen *post mortem* betrouwbaar gemeten worden.

Het was daarom niet mogelijk een longitudinale studie naar verandering van spiervezeloriëntatie uit te voeren. In plaats daarvan is de spiervezeloriëntatie in de infarctharten vergeleken met een referentie van normale spiervezeloriëntatie, verkregen uit andere harten. Voorgaande studies waarin de spiervezeloriëntatie van normale harten is beschreven laten een grote spreiding zien. Deze spreiding wordt deels veroorzaakt door onnauwkeurigheid van de gebruikte histologische meettechniek. Andere oorzaken voor de grote spreiding zijn de problemen die optreden bij het definiëren van een lokaal coördinaatsysteem, en bij detectie van de binnenwand (endocard) van het hart.

In deze studie is een nieuwe meettechniek gebruikt om de spiervezeloriëntatie te bepalen, Magnetic Resonance Diffusion Tensor Imaging (MR-DTI) (hoofdstuk 2). Met behulp van deze techniek is het mogelijk *post mortem* de spiervezeloriëntatie volledig in drie dimensies te bepalen in het intacte hart. Verder is een nieuwe methode ontwikkeld om het lokale coördinaatsysteem te definiëren. Dit coördinaatsysteem is gebaseerd op karakteristieke eigenschappen van het spiervezelveld en kan objectief worden aangebracht. Tenslotte is een nieuwe normalisatiemethode ontwikkeld, waarbij detectie van het endocard niet meer noodzakelijk is. Nadeel van de door ons gebruikte normalizatiemethode is dat offsetverschillen niet gedetecteerd kunnen worden. Op deze manier is het mogelijk gebleken de spiervezeloriëntatie te meten met een nauwkeurigheid van 4.5°, wat beter is dan de 10° die gehaald wordt met histologische methoden. Over vijf verschillende harten gemeten bedroeg de standaarddeviatie 6°. Ook dit is veel beter dan de spreiding die in histologische studies gerapporteerd is.

Vervolgens is onderzocht of de grote spreiding in de gemeten spiervezeloriëntatie, zoals gerapporteerd in literatuur, toegeschreven zou kunnen worden aan verschillen in hartgeometrie (hoofdstuk 3). Daarvoor is met behulp van een numeriek model van de mechanica van de linkerventrikel een schatting gemaakt van de verandering van de spanning die optreedt ten gevolge van geometrievariaties. Vervolgens is gekeken hoeveel de spiervezeloriëntatie zou moeten aanpassen om die spanningsveranderingen te compenseren. Uit deze studie is gebleken dat geometrievariaties zoals die zich in de natuur voordoen, gecompenseerd kunnen worden met aanpassingen in de spiervezeloriëntatie van maximaal 10°. De grote spreiding uit de literatuur kan dus niet aan de geometrieverschillen toegeschreven worden. Waarschijnlijker is dat de grote spreiding het gevolg is van verschillen in de definitie van het coördinaatsysteem.

Vervolgens is de centrale hypothese van dit proefschrift getoetst in een

diermodel (hoofdstuk 4). We hebben ervoor gekozen de lokale mechanica in een geitenhart te verstoren door het aanbrengen van een infarct. Uit literatuur is bekend dat in de randzone rond een infarct de mechanica tijdens systole verstoord is. De spiervezeloriëntatie in de randzone van het infarct is vervolgens tien weken na infarctinductie gemeten met behulp van MR-DTI. Er zijn geen significante verschillen gevonden.
Er zijn een aantal verklaringen mogelijk voor het feit dat geen verschillen in spiervezeloriëntatie zijn gemeten: 1) spiervezels kunnen hun oriëntatie niet aanpassen, of 2) het is niet mogelijk de spanningen in de randzone van het infarct terug te brengen naar normale waarden door adaptatie van de spiervezeloriëntatie, of 3) de spiervezeloriëntatie is wel geadapteerd, maar de aanpassingen die nodig waren zijn niet detecteerbaar.
De eerste mogelijkheid, spiervezels kunnen hun oriëntatie niet aanpassen, wordt weersproken door experimentele gegevens. De overige twee mogelijkheden zijn vervolgens onderzocht met behulp van een numeriek model van de mechanica van de linkerventrikel waarin een infarct was aangebracht (hoofdstuk 5). Met het model werd onderzocht of het mogelijk is de mechanische belasting rondom het infarct homogeen te verdelen door adaptatie van de spiervezeloriëntatie, en zo ja, of de veranderingen in spiervezeloriëntatie die daarvoor nodig zijn ook detecteerbaar zijn. Gebleken is dat de inhomogeniteit van de transmurale aktieve spanning in de randzone van het infarct toenam van 5 tot 15% ten gevolge van de aanwezigheid van het infarct. Deze inhomogeniteit kon worden gecompenseerd door de spiervezelrotatie in de randzone van het infarct in de orde van 10°, waarbij transmuraal dezelfde mate van rotatie nodig was (offset verandering).
We concluderen daaruit dat de hypothese dat verandering van de spiervezeloriëntatie in het hart een adaptief mechanisme is waarmee de belasting van de spiervezels optimaal wordt gehouden, niet mag worden verworpen. De adaptatie van de spiervezeloriëntatie rondom een klein infarct, zoals door ons onderzocht, is echter te klein om met de huidige meet- en analyse technieken gedetecteerd te kunnen worden.

Dankwoord

Onderzoek doe je nooit alleen, en multidisciplinair onderzoek al helemaal niet. Er zijn dan ook veel mensen die een bijdrage hebben geleverd aan de totstandkoming van dit proefschrift. Hen wil ik op deze plaats graag van harte bedanken.
Allereerst natuurlijk Peter Bovendeerd en Theo Arts, die mij met raad en daad ter zijde hebben gestaan. Bedankt voor de brainstormsessies, de discussiebijeenkomsten, de geboden oplosstrategieën, maar bovenal voor de fijne samenwerking. Dick van Campen wil ik bedanken voor het mogelijk maken van deze promotie.
Frits Prinzen heeft meegeholpen met het opzetten van de dierexperimenten en met het analyseren van de gegevens. Maaike Peschar gaf mij ogen en handen in Maastricht, zodat tijdens de experimenten altijd voldoende gesteriliseerde katheters, sheets en dergelijke aanwezig waren. De gouden handjes van Theo van de Nagel, Ruud Krüger en Leo Ennen hebben tijdens de experimenten het echte werk gedaan. Ook hielden ze mijn geitjes altijd wat extra in de gaten, aangezien ik daartoe vanuit Eindhoven niet in staat was. Theo van de Nagel heeft voor mij de hemodynamische data uitgewerkt, zodat we het hemodynamische effect van het aangebrachte infarct in de gaten konden houden. Heel hartelijk bedankt voor al jullie hulp.
De MR-tagging experimenten, die wegens tijdgebrek helaas niet in dit proefschrift opgenomen konden worden, zijn opgezet en uitgewerkt door Annette van der Toorn. Riël Snoep heeft het MR-meetprotocol mee ontwikkeld, en ons ruim meettijd op de klinische scanner gegeven. De MR-laboranten in het AZM, door wie deze metingen zijn uitgevoerd, hebben zich niet af laten schrikken door de afwijkende anatomie van de geit, of door grote storingen op het ECG. Hartelijk bedankt voor jullie inzet.
De MR-DTI experimenten zijn opgezet en uitgevoerd in samenwerking met Klaas Nicolay. Verder hebben Erwin Blezer, Boudewijn van de Sande, Frank ter Veld en Gerard van Vliet geholpen bij het uitvoeren van de MR-DTI

experimenten. De controleharten zijn verzameld door Hans Vosmeer. Ook jullie wil ik hiervoor hartelijk bedanken.
Onze systeembeheerders, Patrick van Brakel en Leo Wouters, wil ik bedanken voor de eerste hulp bij onwillige computers. Al mijn collega's en vooral ook mijn kamergenoten Roy, Hans en Lyosha wil ik bedanken voor de discussies over zinnige, maar vooral ook onzinnige onderwerpen. Roy, bedankt voor het doorlezen van mijn proefschrift en veel succes met het jouwe.
Pap, mam, bedankt voor jullie steun en liefde. En tenslotte, lieve Niels, bedankt voor alles!

Liesbeth Geerts-Ossevoort
Eindhoven, april 2002

Curriculum Vitae

8 november 1973	Geboren te Waalre
1986-1992	Gymnasium-β, Van Maerlantlyceum, Eindhoven
1992-1993	Propedeuse Werktuigbouwkunde, Technische Universiteit Eindhoven
1993-1997	Werktuigkundige Medische Technologie, Technische Universiteit Eindhoven
1997-2002	Assistent in Opleiding, sectie Dynamics & Control technology, Technische Universiteit Eindhoven
2002-	Applicatie specialist MRI, Philips Medical Systems, Best